Thesis

Pressure Induced Crossover from Non-Fermi-Liquid Behavior to Fermi-Liquid Behavior in a Heavy-Fermion Antiferromagnet Ce_7Ni_3

by

Kazunori Umeo

September 1996

contents

Abstract

The pressure dependence of transport, magnetic and thermal properties of a heavy-fermion antiferromagnet Ce_7Ni_3 has been investigated. At ambient pressure, this compound orders antiferromagnetically below T_N = 1.9 K and exhibits a large Sommerfeld coefficient of 9 J/K^2mol f.u. The Ce ions in the three nonequivalent sites are found to be very close to trivalent from L_{III}-XANES (X-ray absorption near edge structure) spectra and magnetic susceptibility measurements. The resistivity and magnetization are strongly anisotropic at temperatures below T_N = 1.9 K. The combination of Kondo effect and crystal-field effect substantially reduces the specific heat, magnetic entropy and magnetic moment in the antiferromagnetic state. The Kondo temperature T_K is estimated to be ~ 5 K from the values of the specific heat jump and of the magnetic entropy at T_N.

With increasing pressure, T_N of Ce_7Ni_3 is substantially suppressed and vanishes near $P_c \approx 0.32$ GPa. Non-Fermi-liquid (NFL) behavior appears around 0.4 GPa in both the specific heat and AC magnetic susceptibility; $C_m/T \propto -\ln T$ and $\chi_{AC} \propto (1- \alpha T^{1/2})$. Thus, Ce_7Ni_3 is found to be the example of the ordered compound showing the NFL behavior near the magnetic instability. Above 0.62 GPa, the normal Fermi-liquid state recovers as indicated by the T-independence of C_m/T and the T^2-dependence of magnetic resistivity. The observed crossover in $C_m(T)$ with pressure is analyzed in terms of two models, the impurity Kondo model with three Kondo temperatures and the SCR theory of spin fluctuations (SF). It is found that the NFL behavior in C_m/T is better described by the SCR theory. The characteristic SF temperature T_0 increases by a factor of 20 for $0.33 \leq P \leq 0.75$ GPa, yielding a large Grüneisen parameter Γ_e = 220 around 0.4 GPa.

1. Introduction

1.1 Phase diagram of Kondo lattice system

Heavy-fermion compounds have been the focus in the field of strongly correlated electron systems. They contain lanthanides such as cerium and ytterbium, and actinides such as uranium and plutonium in regular lattice sites. Many of them order magnetically at low temperatures, although the Kondo effect at each f ion is expected to promote a nonmagnetic ground state.

Doniach proposed phase diagram[1] for the Ce-based Kondo lattice as shown in Fig. 1. The Néel temperature T_N, Kondo temperature T_K and the characteristic temperature T_{RKKY} of the RKKY interaction, are described by a common parameter $|JN(E_F)|$, where J is the exchange coupling between the 4f electron and conduction electrons and $N(E_F)$ is the conduction-band density of states at the Fermi level. In the region of small $|JN(E_F)|$, T_K is lower than T_{RKKY} and the compound undergoes an antiferromagnetic transition. With

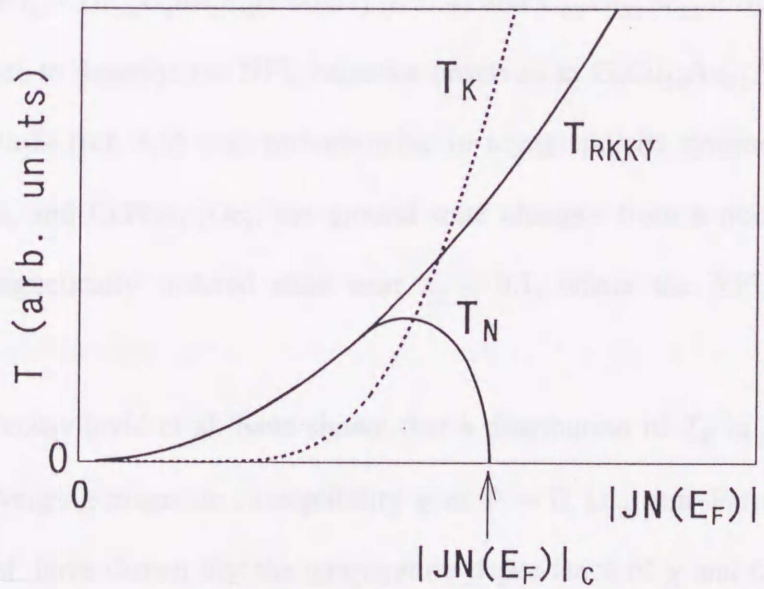

Fig. 1. Schematic phase diagram for a Kondo lattice showing the Néel temperature T_N, the Kondo temperature T_K and the RKKY energy as a function of the product $|JN(E_F)|$ (from ref. 1).

increasing $|JN(E_F)|$, T_K exceeds T_{RKKY} and then the magnetic order is suppressed. When $|JN(E_F)|$ exceeds the critical value $|JN(E_F)|_C$, the ground state becomes nonmagnetic with huge values of Sommerfeld coefficient $\gamma(=C/T(T\rightarrow 0))$, a Pauli-like spin susceptibility χ, and the coefficient A of the T^2-dependence of electrical resistivity ρ with a relation $\gamma \propto \chi \propto A^{1/2}$(ref. 2). The low-temperature properties have been generally described within the framework of the conventional Fermi liquid theory. With further increasing $|JN(E_F)|$, the system becomes an intermediate valence state.

1.2. Non-Fermi-liquid behavior

Recently, non-Fermi-liquid (NFL) behaviors, $C/T \propto -\ln T$, $\chi \propto (1-\alpha T^{1/2})$ and $\Delta\rho \propto T$ have been reported for some U- and Ce-based alloys near $|JN(E_F)|=|JN(E_F)|_C$ when the magnetic state is destroyed by the substitution of the constituent elements. A two-channel Kondo model was proposed to explain the NFL behavior in U-based systems such as $U_{0.2}Y_{0.8}Pd_3$,[3] $Th_{1-x}U_xRu_2Si_2$($x\leq 0.07$) (ref. 4) and $U_{0.9}Th_{0.1}Be_{13}$.[5] However, this model is not adequate to describe the NFL behavior observed in $CeCu_{5.9}Au_{0.1}$,[6] $CePtSi_{0.9}Ge_{0.1}$,[7] and $Ce_{1-x}La_xRu_2Si_2$(ref. 8,9) with orthorhombic or tetragonal site symmetry for Ce^{3+}. In both $CeCu_{6-x}Au_x$ and $CePtSi_{1-x}Ge_x$, the ground state changes from a nonmagnetic state to an antiferromagnetically ordered state near $x_c = 0.1$, where the NFL behavior has been observed.

Dobrosavljević et al. have shown that a distribution of T_K in a disordered systems induces diverging magnetic susceptibility χ as $T \rightarrow 0$, i.e., non-Fermi-liquid behavior.[10] Bernal et al. have shown that the temperature dependence of χ and C of $UCu_{5-x}Pd_x$ are in agreement with the model.[11] The distribution in T_K can be led from fluctuations in the exchange coupling between the 4f and conduction electrons, J, or in the density of state of

conduction electrons, $N(E_F)$.

Moriya and Takimoto have applied the self-consistent renormalization (SCR) theory of spin fluctuations (SF) to the heavy-fermion systems near the antiferromagnetic instability.[12] They have argued that the dynamical susceptibility of the systems mainly due to the f-electrons can be described in terms of mutually interacting local spin fluctuations. According to the SCR theory, the temperature dependence of specific heat and resistivity is represented as a function of the characteristic SF energy T_0.[12] The calculation have shown that the specific heat and resistivity exhibit the temperature variation of the NFL form, $C/T \propto -\ln T$ and $\rho \propto T$ in a certain range of temperature around T_0, and the form, $C/T \propto 1-T^{1/2}$ and $\rho \propto T^{3/2}$ at the critical boundary ($y_0 = 0$). Kambe et al. have used this theory to analyze the data of C and ρ of $Ce_{1-x}La_xRu_2Si_2$ [8,9] and $CeCu_{6-x}Au_x$,[9] and have argued that the NFL behavior is the consequence of antiferromagnetic SF of 4f electrons with characteristic energy much smaller than that in itinerant 3d-electron systems. They have pointed out further that the lattice disorder introduced by the alloying must be taken into account, because the SCR theory assumes a perfect lattice. Therefore, a systematic study of physical properties near the magnetic instability is desired by using a heavy-fermion compound with an ordered crystal structure. In this respect, we should recall that for magnetically ordered Ce compounds in the region $|JN(E_F)| < |JN(E_F)|_C$, pressure increases hybridization and thus moves the system to the larger $|JN(E_F)|$ region.[13] Indeed, the pressure-induced transition from antiferromagnetic to nonmagnetic state has been found in several compounds, e.g., $CeIn_3$ (ref. 14), $CeRh_2Si_2$ (ref. 15) and $CeCu_2Ge_2$ (ref. 16). More recently, for the antiferromagnetic heavy-fermion alloy $CeCu_{5.7}Au_{0.3}$ ($T_N = 0.49$ K for $P = 0$), the NFL behavior in $C(T)$ was observed at the critical pressure $P_c = 0.82$ GPa where T_N vanishes.[17]

1.3. Structural and magnetic properties of Ce_7Ni_3

In the Ce–Ni binary phase diagram, there exist 6 ordered compounds, which show various magnetic and electronic properties. The cerium in $CeNi_5$ and CeNi possesses the intermediate valence state,[18] leading to a nonmagnetic ground state. On the other hand, Ce_7Ni_3 orders antiferromagnetically below 1.8 K.[18] Sereni et al. have found that the magnetic order coexists with a heavy fermion state.[19] Figure 2(a) shows the temperature dependence of specific heat divided by temperature C_p/T in a magnetic fields. A large value of γ = 9 J/K^{2}mol f.u. is obtained from the extrapolation to T = 0 K at B = 0. While the anomaly around 1.6 K is due to the antiferromagnetic order, the origin of the anomaly near 0.4 K has not been elucidated yet. The anomaly at the lower temperature is also observed in χ_{AC} as shown in Fig. 2(b).[19]

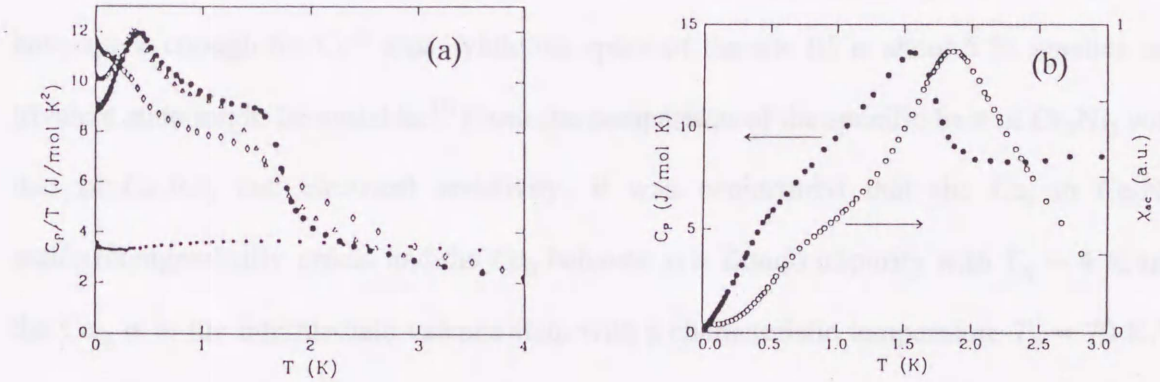

Fig. 2. (a) Specific heat divided by the temperature C_p/T vs. T for Ce_7Ni_3 in magnetic fields B = 0 T(●), 0.2 T(△), 0.5 T(◇) and 6 T(■), and (b) specific heat (●) and AC magnetic susceptibility (○) vs. T (from ref. 19).

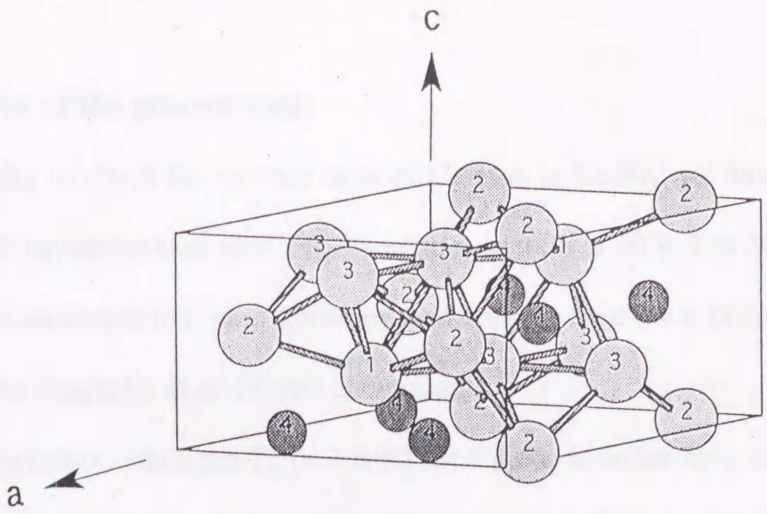

Fig. 3. The hexagonal Th_7Fe_3–type structure for Ce_7Ni_3. The circles 1,2,3 and 4 stand for Ce_I, Ce_{II}, Ce_{III} and Ni, respectively.

Ce_7Ni_3 crystallizes in the hexagonal Th_7Fe_3–type structure (space group $P6_3mc$) as shown in Fig. 3.[20] There are three nonequivalent crystallographic Ce sites (I,II, and III). The site I (1 Ce atom) has trigonal symmetry (point group C_{3v}), and both site II (3 Ce atoms) and III (3 Ce atoms) have monoclinic symmetry (point group C_{1v}). Sites I and II have space enough for Ce^{3+} ions, while the space of the site III is about 5 % smaller and trivalent state might be unstable.[19] From the comparison of the specific heat of Ce_7Ni_3 with that of Ce_7Rh_3 and electrical resistivity, it was conjectured that the Ce_I in Ce_7Ni_3 antiferromagnetically orders and the Ce_{II} behaves as a Kondo impurity with $T_K \approx 4$ K and the Ce_{III} is in the intermediate valence state with a characteristic temperature $T_0 \approx 70$ K.[19] However, from the measurement of Ce L_{III}–XANES spectra at 300 K, Neifeld et al. showed that the valence of Ce in Ce_7Ni_3 was 3.03.[21] Furthermore, from the Ce 3d X–ray photoelectron spectroscopy (XPS) (ref. 22) and bremsstrahlung isochromat spectroscopy (BIS),[23] the relative intensities of the "f^0" peaks in spectra were estimated to be < 0.05 and 0.02 ~ 0.08, respectively. These results suggest that the valence of all the Ce ions in Ce_7Ni_3 is close to 3.

1.4. Purpose of the present study

In order to check the valence state of Ce ions in Ce_7Ni_3, we have measured Ce L_{III}–XANES (X–ray absorption near edge structure) spectra at $10 \leq T \leq 300$ K. Measurements of magnetic susceptibility, magnetization and specific heat have been performed in order to clarify the magnetic state of this compound.

Furthermore, since the T_N (= 1.8 K) for Ce_7Ni_3 is rather low, it is expected that the antiferromagnetism can be destroyed by the application of pressure in the accessible range. Near the transition from magnetic to nonmagnetic state, we also anticipate that the non–Fermi–liquid behavior appears. As a matter of fact, the pressure induced transition has been found by the measurements of specific heat, AC magnetic susceptibility and electrical resistivity under pressures.

In the following, the method of sample preparation and experiments are described in Chapter 2. The experimental results are presented in Chapter 3. In Chapter 4, we analyze and discuss the pressure dependence of the physical properties of Ce_7Ni_3 in terms of the SCR theory of spin fluctuations and the impurity Kondo model with distributed Kondo temperatures.

2. Experimental procedure

2.1. Sample preparation

Ingots of Ce_7Ni_3 and La_7Ni_3 were prepared by arc melting of the starting materials under an argon atmosphere. Starting materials of Ce and La were 99.9% and Ni was 99.99% in purity. The X-ray powder diffraction pattern of as grown samples with initial stoichiometry of $Ce_{7.00}Ni_{3.00}$, $Ce_{7.07}Ni_{2.93}$, and $Ce_{7.14}Ni_{2.86}$ are shown in Fig. 4. It is found that $Ce_{7.07}Ni_{2.93}$ is single phase of the Th_7Fe_3 type structure, while $Ce_{7.00}Ni_{3.00}$ and $Ce_{7.14}Ni_{2.86}$ contain CeNi phase(CrB-type orthorhombic structure)(ref. 24) and γ-Ce(fcc structure)(ref. 25) as the second phases, respectively. More detailed analysis of X-ray diffraction indicated that single phase sample was obtained in the starting composition range from 7.05 : 2.95 to 7.10 : 2.90. From EPMA (electron probe micro-analysis), it was found that the ratio of Ce and Ni in the matrix of both $Ce_{7.05}Ni_{2.95}$ and $Ce_{7.07}Ni_{2.93}$ was 7.00 : 3.00 within the relative accuracy (± 0.03) of EPMA. In both samples Ce oxides were found as impurity phase which corresponds to an excessive amount of Ce. This fact suggests that the excess Ce becomes oxides due to oxygen contained in the starting Ce metal. In this work, an excess Ce and La by about 2at.% was added to obtain single-phase samples. The alloy ingots were homogenized by annealing in vacuum at 400°C for 7 days. By powder X-ray analysis, the lattice constants *a* and *c* of Ce_7Ni_3 were determined to be 9.936(1) Å and 6.314(1) Å, respectively, in good agreement with the values reported.[26] A single crystal of Ce_7Ni_3 was grown by a Czochralski method using a hot tungsten crucible in a radio-frequency furnace. The crystal orientation was determined by the back Laue method.

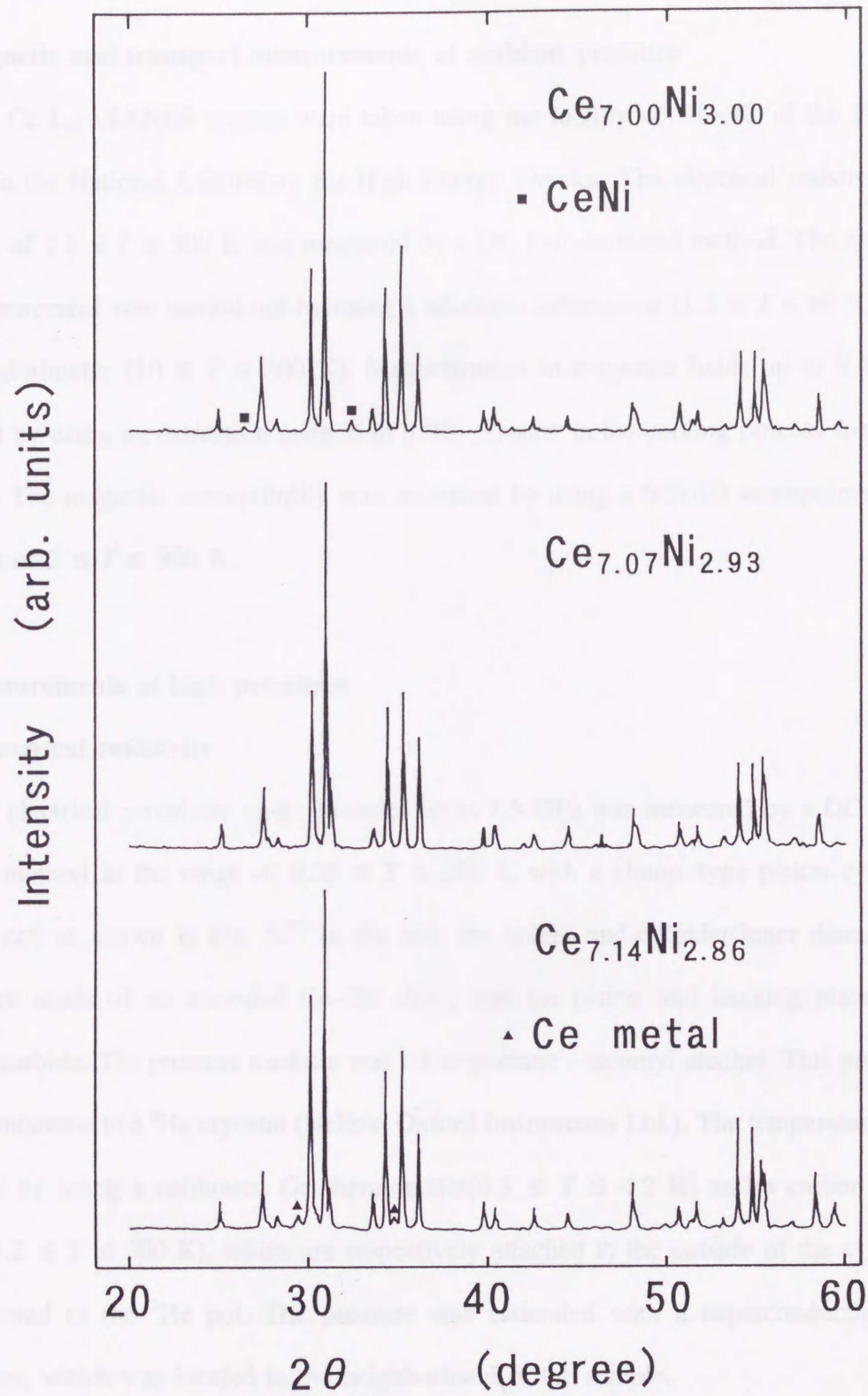

Fig. 4. Powder X-ray diffraction profiles of the samples with nominal compositions $Ce_{7.00}Ni_{3.00}$, $Ce_{7.07}Ni_{2.93}$ and $Ce_{7.14}Ni_{2.86}$ using Cu K_α radiation.

2.2. Magnetic and transport measurements at ambient pressure

The Ce L_{III}–XANES spectra were taken using the facility of BL–7C of the Photon Factory in the National Laboratory for High Energy Physics. The electrical resistivity in the range of $1.5 \leq T \leq 300$ K was measured by a DC four–terminal method. The specific heat measurement was carried out by using a adiabatic calorimeter ($1.3 \leq T \leq 60$ K), and an AC calorimeter ($10 \leq T \leq 300$ K). Magnetization in magnetic fields up to 8 T was measured by using an extraction method in a ^{3}He cryostat in the cooling process from 4.2 to 0.5 K. The magnetic susceptibility was measured by using a SQUID susceptometer in the range of $2 \leq T \leq 300$ K.

2.3. Measurements at high pressures

2.3.1. Electrical resistivity

The electrical resistivity under pressure up to 1.5 GPa was measured by a DC four–terminal method in the range of $0.35 \leq T \leq 300$ K with a clamp–type piston cylinder pressure cell as shown in Fig. 5.[27] In the cell, the holder and cylinder(inner diameter 6 mm) were made of an annealed Cu–Be alloy, and the piston and backing plate of a tungsten carbide. The pressure medium was 1:1 n–pentane – isoamyl alcohol. This pressure cell was mounted to a ^{3}He cryostat (Heliox, Oxford Instruments Ltd.). The temperature was measured by using a calibrated Ge thermometer($0.3 \leq T \leq 4.2$ K) and a carbon glass resistor($4.2 \leq T \leq 300$ K), which are respectively attached to the outside of the cylinder and mounted to the ^{3}He pot. The pressure was estimated with a superconducting Pb manometer, which was located in the neighborhood of the sample.

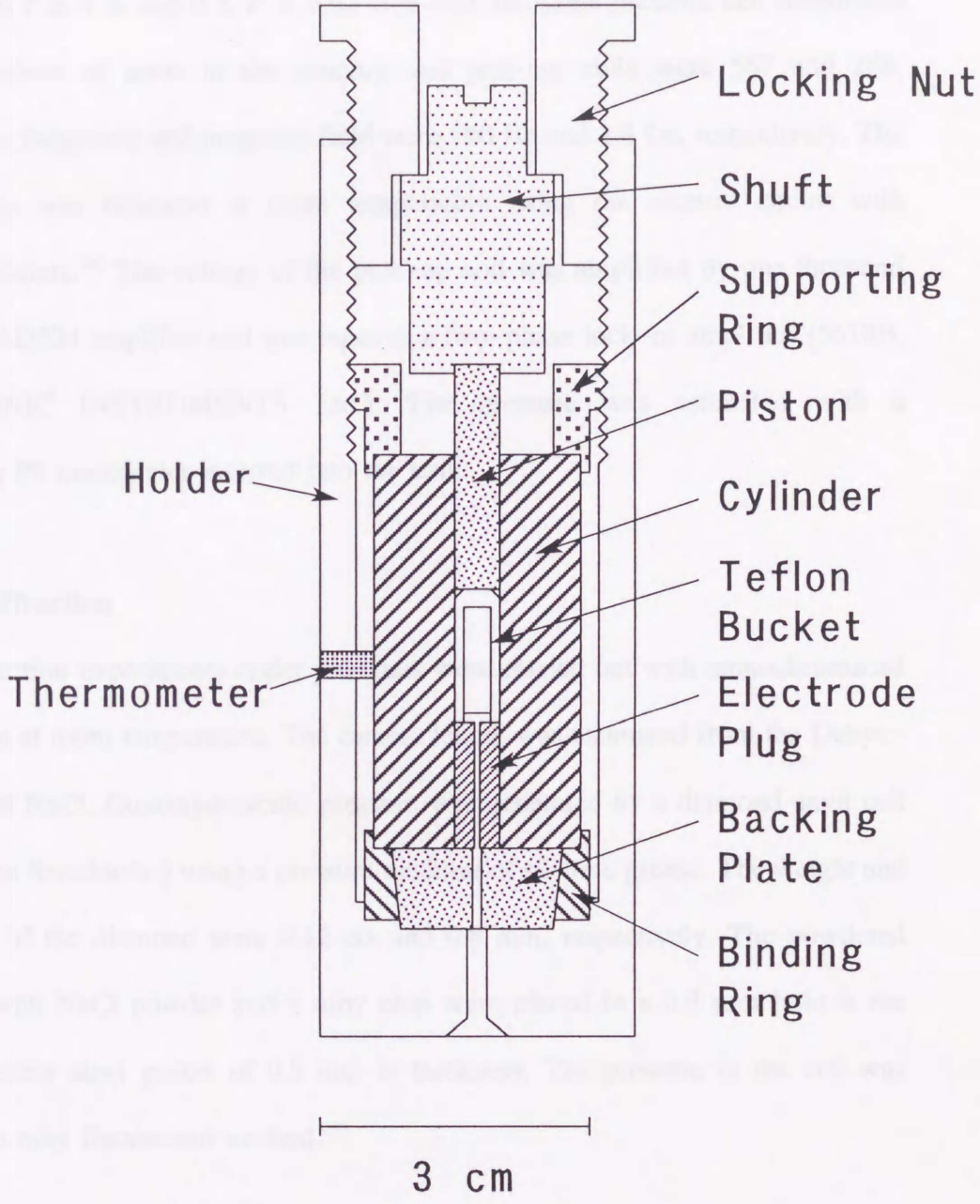

Fig. 5. Clamp-type piston cylinder pressure cell (from ref. 27).

2.3.2. AC magnetic susceptibility

The measurement of χ_{AC} was performed by means of the Hartshorn bridge in the ranges of $0.35 \leq T \leq 4$ K and $0 \leq P \leq 0.62$ GPa with the same pressure cell mentioned above. The numbers of turns in the primary and pick-up coils were 567 and 288, respectively. The frequency and magnetic field were 100 Hz and 1.8 Oe, respectively. The Hartshorn bridge was balanced at room temperature using the electric circuit with operational amplifiers.[28] The voltage of the pick-up coil was amplified by one thousand times using an AD524 amplifier and was input to a two-phase lock-in amplifier (5610B, NF ELECTRONIC INSTRUMENTS Ltd.). The pressure was estimated with a superconducting Pb manometer inserted into the coil.

2.3.3. X-ray diffraction

X-ray diffraction experiments under pressures were carried out with monochromaced Mo $K\alpha$ radiation at room temperature. The camera length was estimated from the Debye-Scherrer rings of NaCl. Quasihydrostatic pressure was generated by a diamond anvil cell (MK 50, Shimizu Seisakusho) using a pressure medium of silicone grease. The weight and culet diameters of the diamond were 0.12 cts and 0.8 mm, respectively. The powdered sample mixed with NaCl powder and a ruby chip were placed in a 0.3 mm hole at the center of a stainless steel gasket of 0.5 mm in thickness. The pressure in the cell was determined by a ruby fluorescent method.[29]

2.3.4 Specific heat

The heat capacity C up to 0.75 GPa was measured using the AC method adapted for a high pressure studies.[30] The sample, a thermometer of RuO_2 and a heater of moleculoy

wire were lapped together in an indium sheet. By measuring the total heat capacity of Ce_7Ni_3 (3.22 mg) and the In sheet (20.31 mg), we calibrated both the pressure and the absolute value of $C(T)$; the former was determined from the known pressure dependence of the superconducting transition temperature $T_c(P)$ of In, $dT_c/dP = -0.42$ K/GPa,[31] and the latter from the jump of C at T_c.[32]

3. Experimental Results

3.1. Physical properties of Ce_7Ni_3 at ambient pressure

3.1.1. Ce L_{III}-XANES

The L_{III}-XANES(X-ray absorption near edge structure) has been used widely to assess the valence of Ce in many heavy-fermion and intermediate valence compounds.[33] The $2p_{3/2}$ (L_{III}) absorption, which favors a $2p_{3/2} \rightarrow 5d$ transition by a $\Delta l = \pm 1$ selection rule, leads to two possible final states,

$$|2p^5...4f^1\ 5d^1\ 6s^2\rangle, \qquad |2p^5...4f^0\ 5d^2\ 6s^2\rangle.$$

The are separated in energy by about 9 eV because the core hole attracts $4f^1$ configuration more than the $4f^0$.(ref. 34) There will be two absorption peaks (white lines) in the L_{III} spectra, and the relative intensities give a determination of the valence. In fact, for the intermediate valence compounds such as $CeNi_2$, $CeNi_5$ and $CePd_3$, two white lines have been observed.[33]

Figure 6 shows Ce L_{III}-XANES spectra for Ce_7Ni_3 at 300, 200, 100 and 10 K, after the back ground was subtracted. The fitted line was obtained by using a functional form of the sum of a Lorentzian representing transition from the Ce $2p_{3/2}$ level into empty Ce 5d states above the Fermi energy plus an arctangent step representing transitions to final states in the continuum. In the present spectra of Ce_7Ni_3, a single peak of L_{III} edge is seen. This fact suggests that the valence of all the Ce ions in Ce_7Ni_3 is close to 3 over the temperature range.

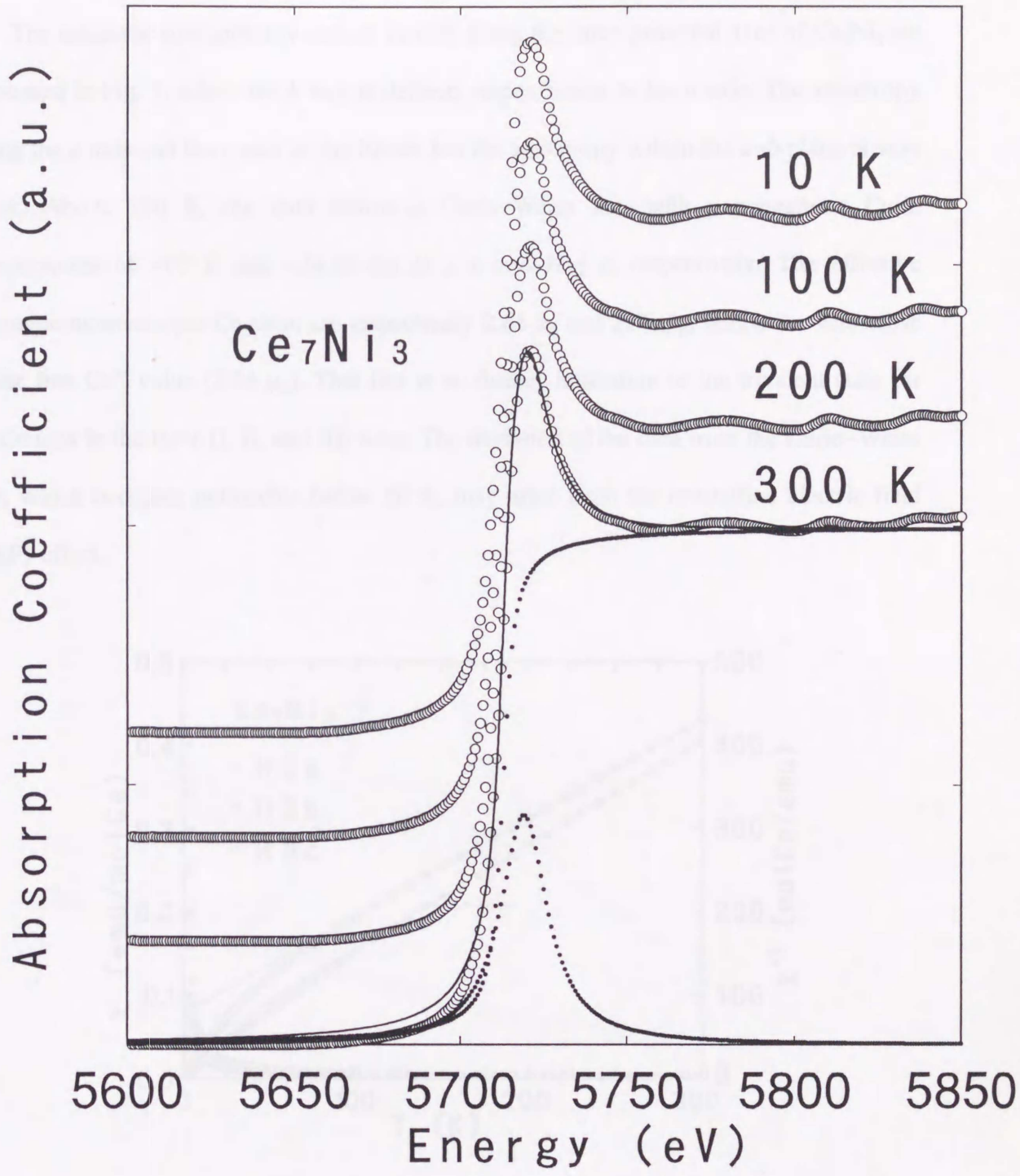

Fig. 6. Ce L_{III}–XANES spectra of Ce_7Ni_3 at 300, 200, 100 and 10K. The dotted lines show a Lorentzian and an arctangent step.

3.1.2 Magnetic susceptibility

The magnetic susceptibility and its inverse along the three principal axes of Ce_7Ni_3 are presented in Fig. 7, where the *b* axis is defined perpendicular to the *a* axis. The anisotropy along the *a* axis and the *c* axis is significant but the anisotropy within the *a*–*b* plane is very weak. Above 100 K, the data follow a Curie–Weiss law with paramagnetic Curie temperatures of −67 K and −24 K for $H \perp c$ and $H \parallel c$, respectively. The effective magnetic moments per Ce atom are respectively 2.61 μ_B and 2.52 μ_B, which are very close to the free Ce^{3+} value (2.54 μ_B). This fact is an further indication of the trivalent state for all Ce ions in the three (I, II, and III) sites. The deviation of the data from the Curie–Weiss law, which becomes noticeable below 50 K, may arise from the crystalline electric field (CEF) effect.

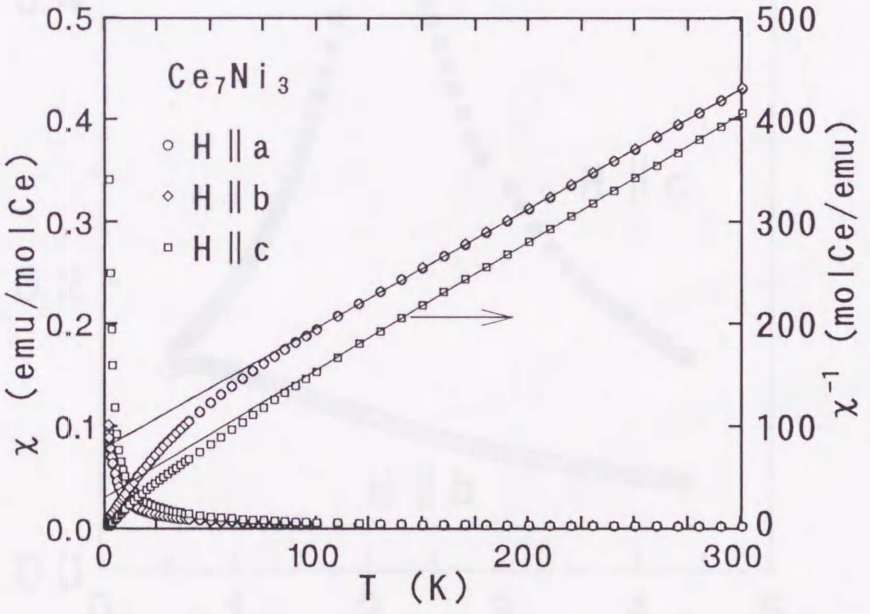

Fig. 7. DC magnetic susceptibility and the inverse along the *a*, *b*, and *c* axes of Ce_7Ni_3 single crystal, where the *b* axis is defined as perpendicular to the *a* axis.

3.1.3 Magnetization

The thermal variation of the magnetization divided by the external field of 0.05 T along the *b* and *c* axes is presented in Fig. 8. For $H \parallel c$, the temperature where $d(\chi T)/dT$ has the maximum value agrees with T_N = 1.8 K determined from the peak in C_m. The broad maximum at 0.6 K for $H \parallel b$ resembles with the previous data obtained for a polycrystalline sample, suggesting the presence of another magnetic transition. The field dependence of magnetization along the *b* and *c* axes at 4.2 K, 1.2 K and 0.5 K are

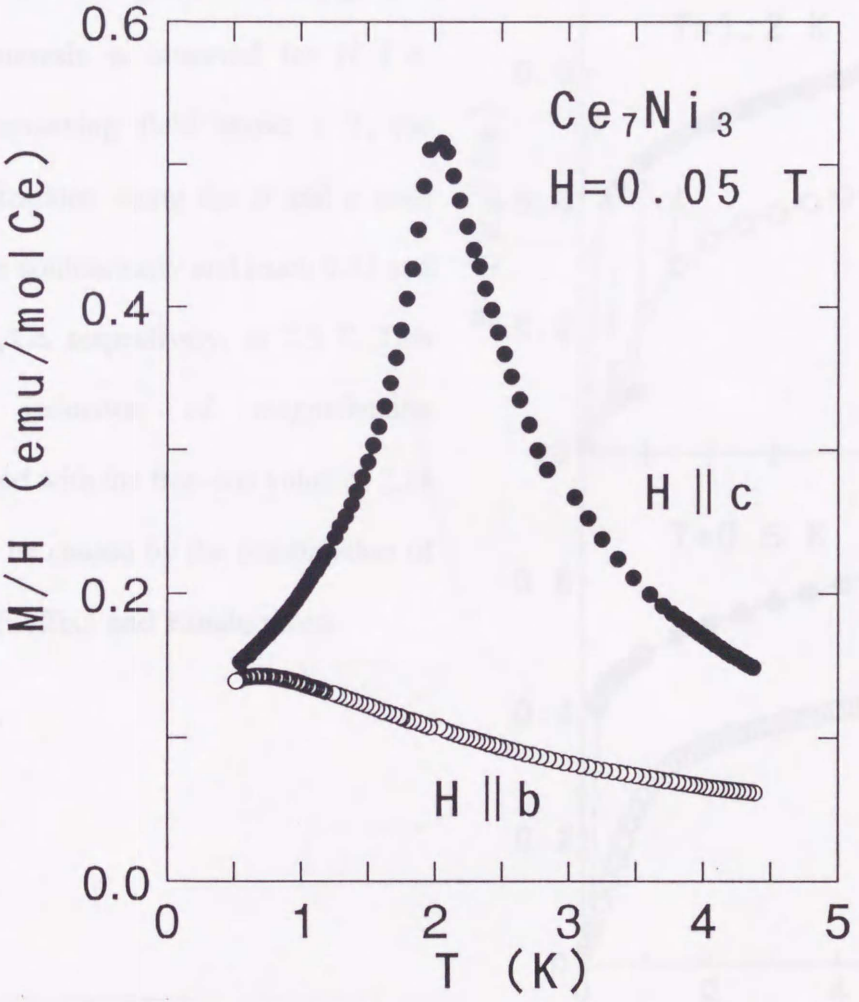

Fig. 8. Magnetization divided by the external field *M*/*H* vs. temperature of Ce_7Ni_3 for $H \parallel b$ and $H \parallel c$ at 0.05 T.

presented in Figs. 9(a), 9(b) and 9(c),respectively. The magnetization was measured in the cooling process. In the virgin run for $H \parallel c$ at 1.2 K, the magnetization exhibits a hysteresis. In the second run, however, the metamagnetic transition occurs at 0.1 T for both increasing and decreasing field. No hysteresis is observed for $H \parallel b$. With increasing field above 1 T, the magnetizations along the b and c axes increase continuously and reach 0.55 and 0.68 μ_B/Ce, respectively, at 7.5 T. This strong reduction of magnetization compared with the free-ion value of 2.14 μ_B may be caused by the combination of the CEF effect and Kondo effect.

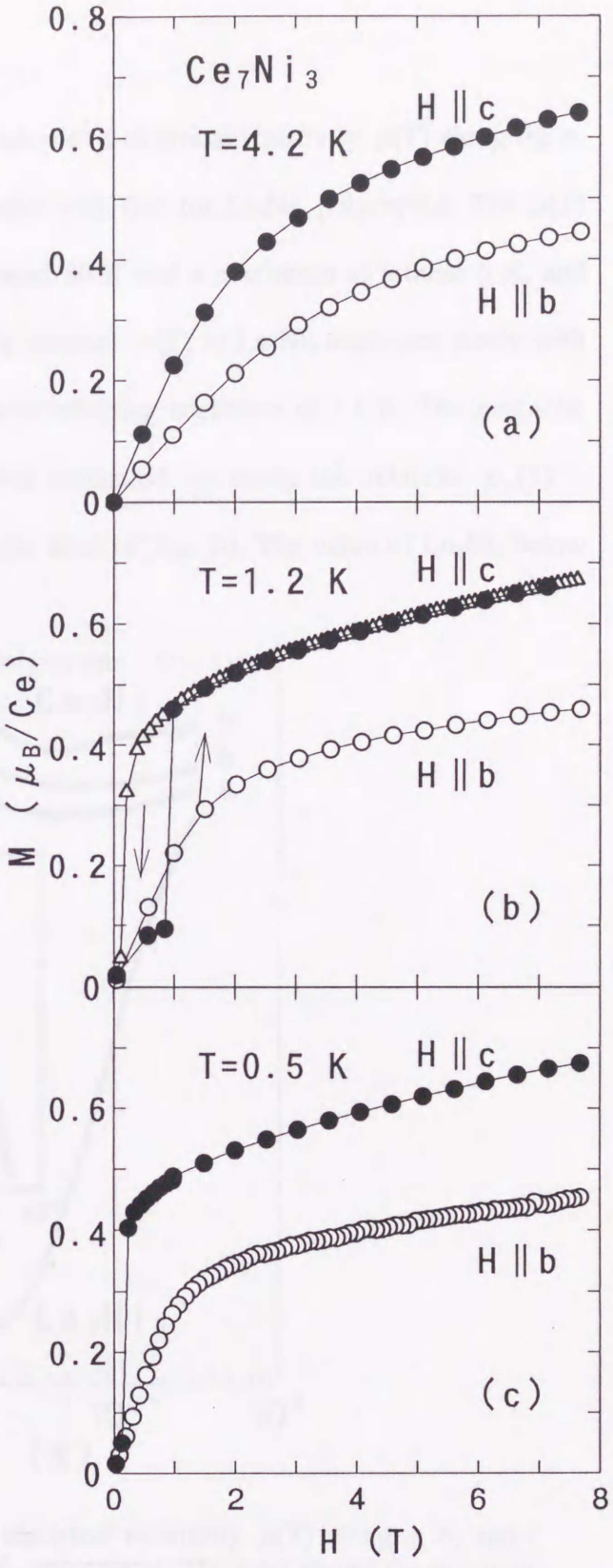

Fig. 9. Field dependence of magnetization of Ce_7Ni_3 along b and c axes at 4.2 K(a), 1.2 K(b) and 0.5 K(c).

3.1.4. Electrical resistivity

Figure 10 shows the temperature dependence of electrical resistivity $\rho(T)$ along the *a*, *b*, and *c* axes of Ce_7Ni_3 single crystal together with that for La_7Ni_3 polycrystal. The $\rho(T)$ along the three axes has a minimum at around 50 K and a maximum at around 6 K, and remains to be 120 ~ 130 $\mu\Omega$cm at 1.4 K. By contrast, $\rho(T)$ of La_7Ni_3 decreases steely with decreasing temperature, and exhibits a superconducting transition at 2.1 K. The magnetic contribution to $\rho(T)$ from 4f electrons was estimated by using the relation, $\rho_m(T) = \rho(Ce_7Ni_3) - \rho(La_7Ni_3)$, which is shown in the inset of Fig. 10. The value of La_7Ni_3 below

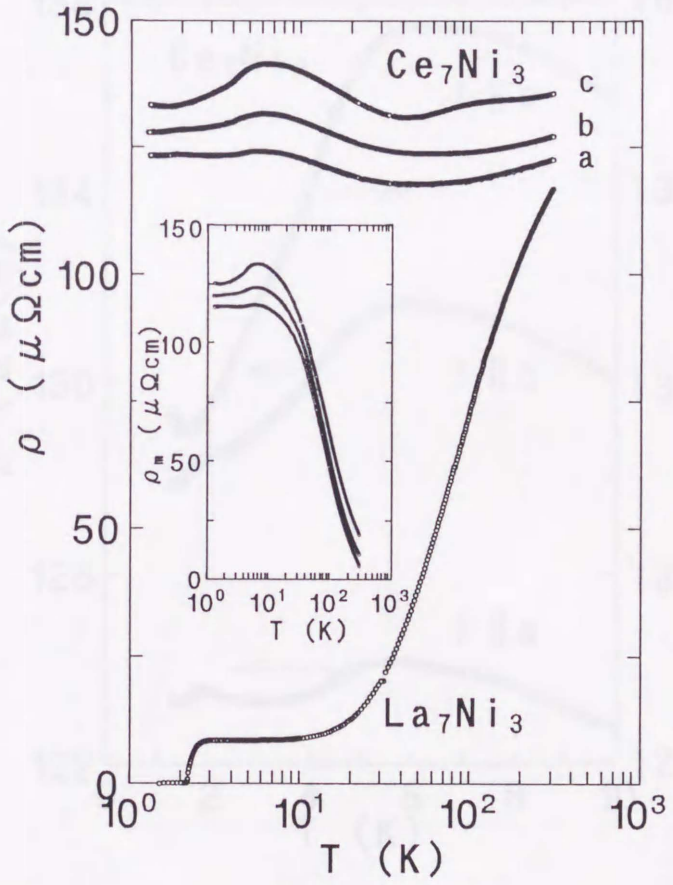

Fig. 10. Temperature dependence of electrical resistivity $\rho(T)$ along *a*, *b*, and *c* axes of Ce_7Ni_3 single crystal and La_7Ni_3 polycrystal. The inset shows the magnetic contribution ρ_m vs. log*T*.

2.1 K was evaluated by the extrapolation of $\rho(T)$ data from 10 K to 3 K. Thus obtained $\rho_m(T)$ for $T \geq 50$ K is proportional to $-\ln T$, which is characteristic of so-called "dense Kondo system". The low-temperature part of $\rho(T)$ is shown in Fig. 11. The maximum in ρ at 6 K is considered to be the onset of coherent scattering of conduction electrons from periodically arrayed Ce ions. It is noteworthy that $\rho(T)$ for $I \parallel c$ turns up below T_N whereas magnetic scattering usually decreases below T_N. This fact suggests that the antiferromagnetic order creates a partial gap along the c axis on the Fermi surface.

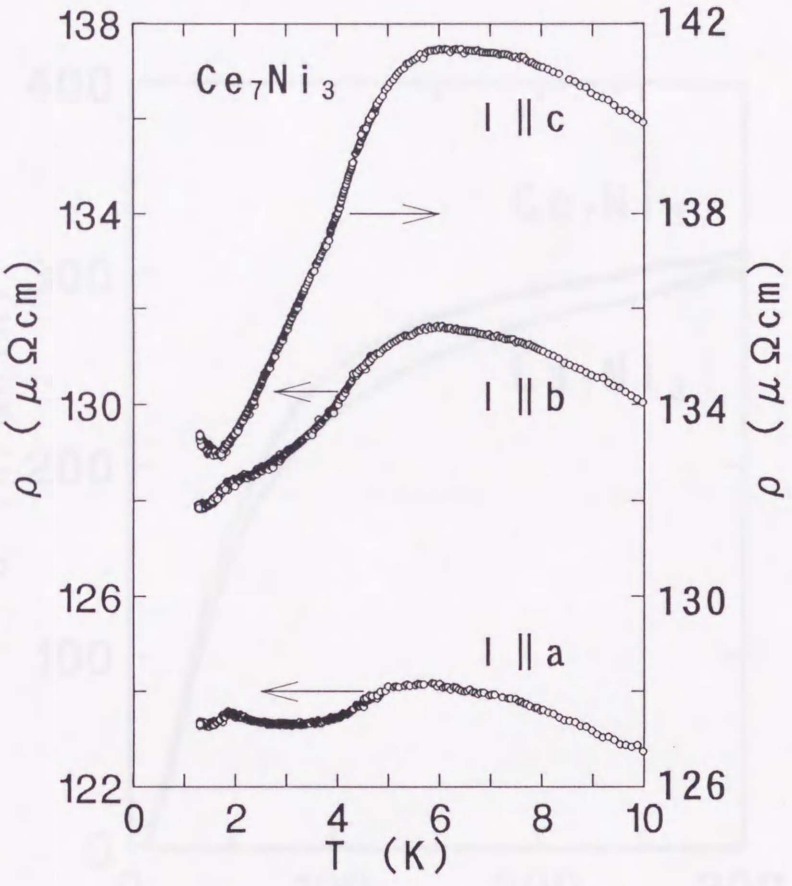

Fig. 11. Electrical resistivity of Ce_7Ni_3 along the three principal axes.

3.1.5. Specific heat

The temperature dependence of the specific heat of Ce_7Ni_3 and La_7Ni_3 is shown in Fig. 12. In order to estimate the magnetic contribution C_m, the value of C for La_7Ni_3 was subtracted from that for Ce_7Ni_3. Thus obtained C_m/T per Ce atom is plotted in Fig. 13(a) as a function of T (on a logarithmic scale). A λ−type and Schottky anomalies appear at T_N = 1.8 K and 100 K, respectively. The large part of C_m in the range 2 < T < 50 K may be dominated by the Kondo effect. The specific heat jump at T_N is δC = 1.5 J/molK, which is much smaller than 12.48 J/molK that expected for a magnetic conventional S=1/2 two−level system.

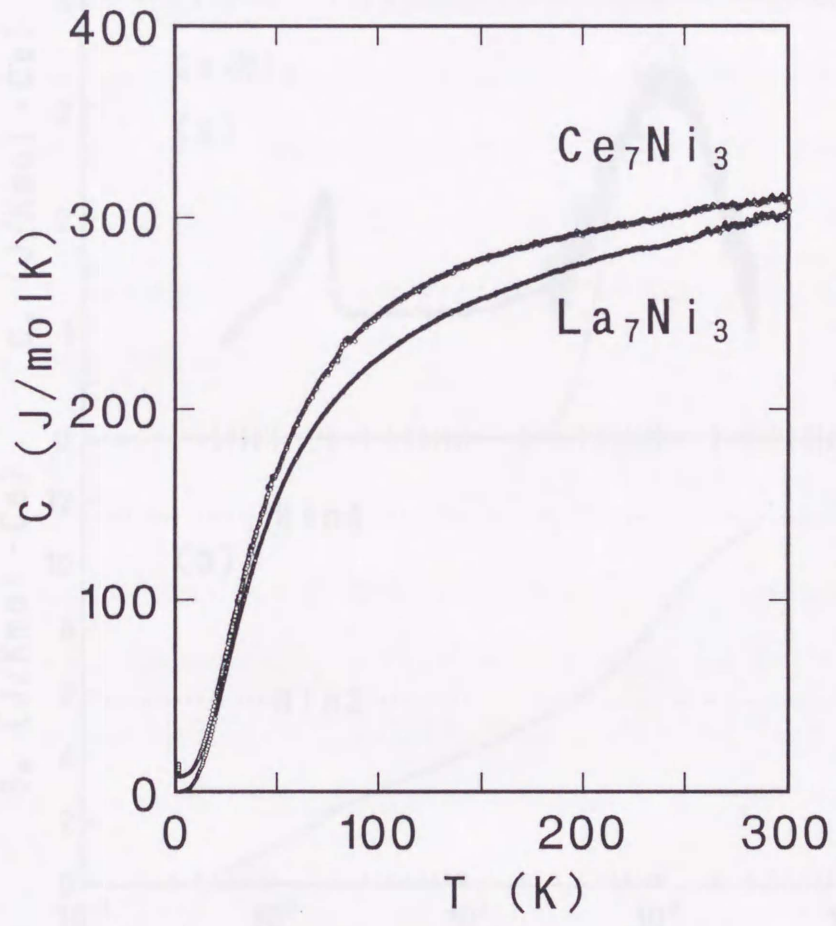

Fig. 12. Temperature dependence of the specific heat of Ce_7Ni_3 and La_7Ni_3.

The temperature dependence of the 4f–derived entropy S_m is shown in Fig. 13(b). We estimated the value of C_m below 0.5 K by extrapolating linearly the data between 0.5 K and 1 K. The entropy gain associated with the magnetic transition is 47 % of Rln2 at the peak position, and reaches Rln2 only at 35 K. The reduced magnetic entropy is a result of the Kondo effect.

The entropy at 300 K is saturated to Rln4 expected for Ce^{3+} ions with the first excited doublet in the CEF level scheme. In Fig. 13(a), the solid line shows the Schottky contribution for the CEF splitting energy of 240 K. The calculated result reproduces the experimental data in the temperature range T > 60 K.

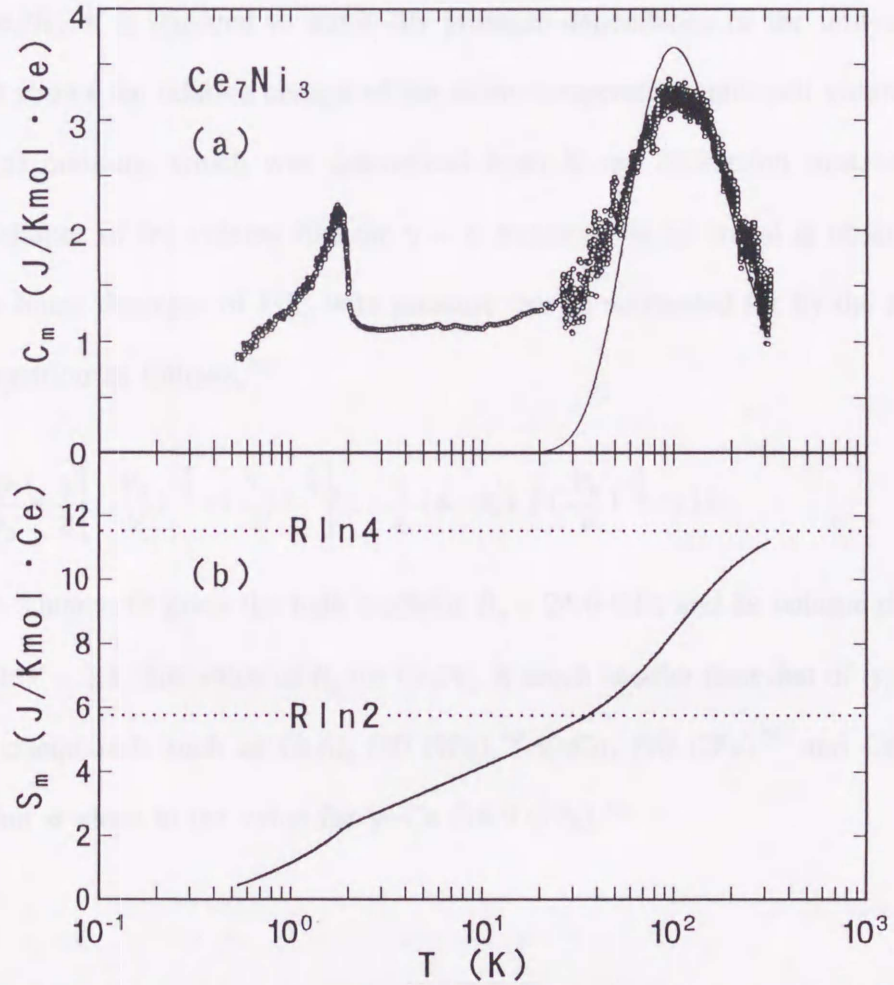

Fig. 13. (a)Temperature dependence of magnetic contribution to specific heat C_m. The solid line shows the Schottky contribution for the energy splitting of 240 K between the ground state and the first excited state. (b)Temperature dependence of the magnetic entropy S_m.

3.2. Physical properties of Ce_7Ni_3 at high pressures

It is natural to expect that the antiferromagnetically ordered state of Ce_7Ni_3 disappears under pressure. Thereby, we anticipate non-Fermi-liquid behavior to appear. Keeping this in mind, we have studied pressure effects on the unit-cell volume, AC magnetic susceptibility $\chi_{AC}(T)$, specific heat $C(T)$, and electrical resistivity $\rho(T)$. The results are presented in the following.

3.2.1. Unit-cell volume

In order to examine the volume dependence of characteristic temperatures of T_N and T_K for Ce_7Ni_3, it is required to know the pressure dependence of the unit-cell volume. Figure 14 shows the relative change of the room-temperature unit-cell volume V/V_0 as a function of pressure, which was determined from X-ray diffraction measurements. No sudden collapse of the volume like the $\gamma - \alpha$ transition in Ce metal is observed up to 7 GPa. The linear decrease of V/V_0 with pressure can be accounted for by the Murnaghan-Birch's equation as follows,[35]

$$\frac{P}{B_0} = \frac{3}{2}\left[\left(\frac{V_0}{V}\right)^{\frac{7}{3}} - \left(\frac{V_0}{V}\right)^{\frac{5}{3}}\right]\left\{1 - \frac{3}{4}\left(4 - B_0'\right)\left[\left(\frac{V_0}{V}\right)^{\frac{2}{3}} - 1\right]\right\}. \qquad (1)$$

The least-squares fit gives the bulk modulus B_0 = 24.6 GPa and its volume derivative $B_0' = d\ln B_0/d\ln V$ = 2.1. The value of B_0 for Ce_7Ni_3 is much smaller than that of typical heavy-Fermion compounds such as $CeAl_3$ (50 GPa),[36] $CeCu_6$ (90 GPa),[36] and $CeInCu_2$ (97.2 GPa),[37] but is close to the value for γ-Ce (18.9 GPa).[38]

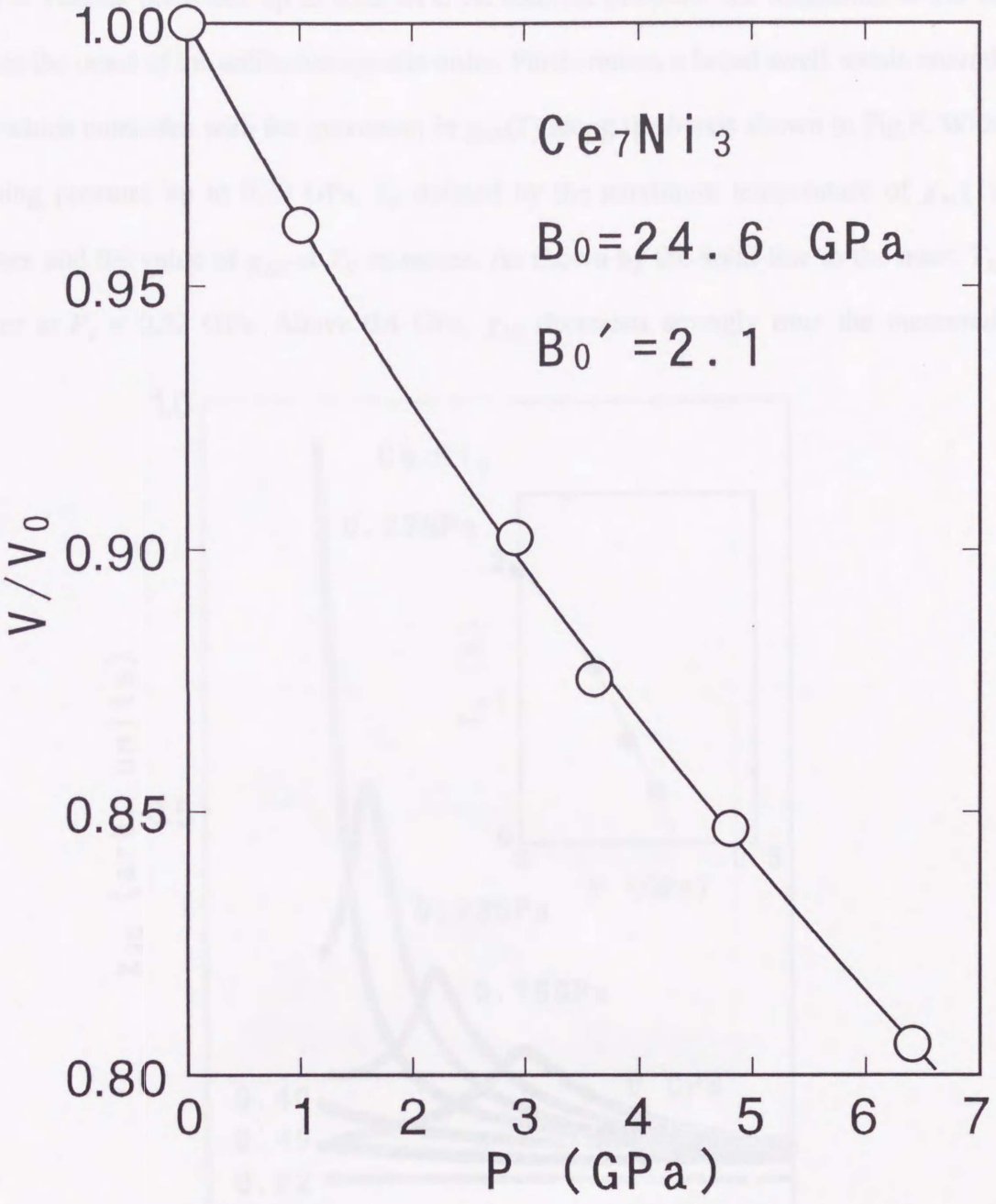

Fig. 14. Relative change of the volume V/V_0 of Ce_7Ni_3 as a function of pressure. The solid line is the fit to the Murnaghan–Birch's equation.

3.2.2. AC magnetic susceptibility

Figure 15 shows the temperature dependence of $\chi_{AC}(T)$ of a polycrystalline sample of Ce_7Ni_3 at various pressures up to 0.62 GPa. At ambient pressure, the maximum at 1.9 K indicates the onset of the antiferromagnetic order. Furthermore, a broad swell exists around 0.6 K, which coincides with the maximum in $\chi_{DC}(T)$ along the b axis shown in Fig.8. With increasing pressure up to 0.29 GPa, T_N defined by the maximum temperature of $\chi_{AC}(T)$ decreases and the value of χ_{AC} at T_N increases. As shown by the solid line in the inset, T_N vanishes at P_c = 0.32 GPa. Above 0.4 GPa, χ_{AC} decreases strongly over the measured

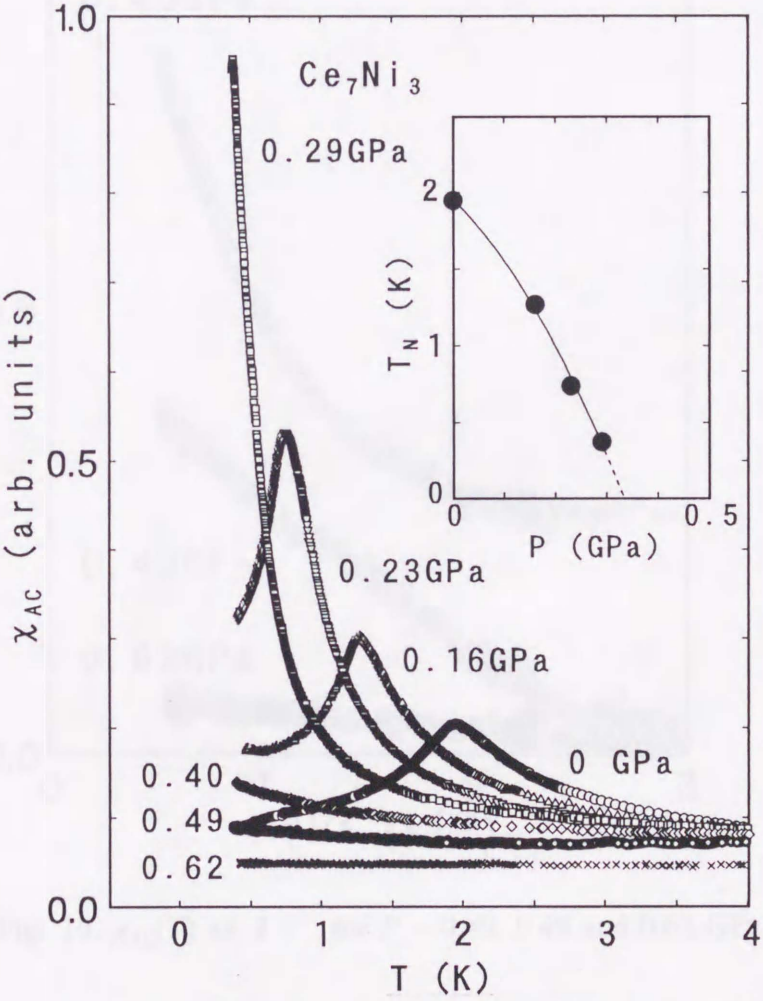

Fig. 15. Temperature dependence of AC magnetic susceptibility χ_{AC} of polycrystalline Ce_7Ni_3 at various pressures. The inset shows the pressure dependence of antiferromagnetic ordering temperature T_N.

temperature range. In order to trace the transition from the NFL behavior to Fermi-liquid behavior, we present in Fig. 16 the data of χ_{AC} vs $T^{1/2}$ at selected pressures between 0.40 GPa and 0.62 GPa. At 0.40 GPa, the NFL behavior, $\chi_{AC} \propto (1-\alpha T^{1/2})$, is observed only below 1 K, while at 0.49 GPa it is observed up to 5 K. At 0.62 GPa, χ_{AC} becomes almost independent of temperature, indicating the recovery of Fermi-liquid behavior.

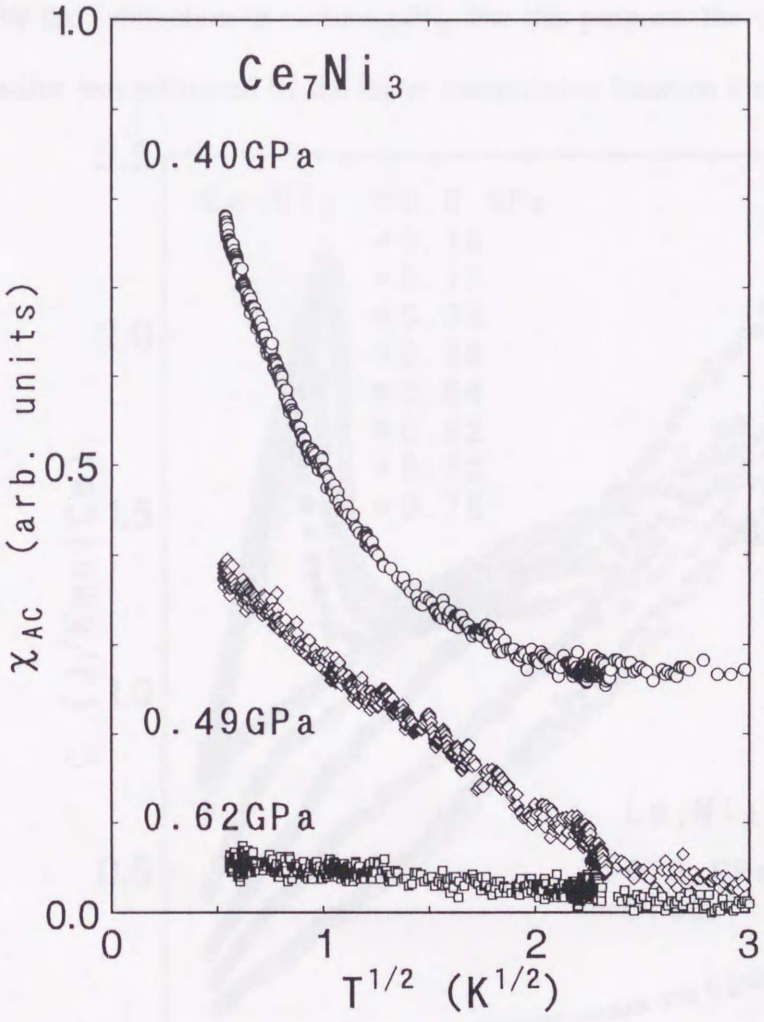

Fig. 16. $\chi_{AC}(T)$ vs. $T^{1/2}$ for P = 0.40, 0.49 and 0.62 GPa

3.2.3. Specific heat

Figure 17 shows $C(T)$ of Ce_7Ni_3 and La_7Ni_3 at various pressures. For $P = 0$, a λ-type anomaly appears at $T_N = 1.8$ K. With increasing pressure, both the specific heat jump $\Delta C(T_N)$ and T_N decrease and vanish at P_c. The pressure dependence of T_N will be discussed in the next section. The $C(T)$ at low temperatures decreases steeply with pressure, while that of La_7Ni_3 hardly changes. The magnetic contribution to the specific heat C_m was estimated by the subtraction of C for La_7Ni_3. For this purpose, the value of C for La_7Ni_3 under pressures was estimated by the linear interpolation between the two values at 0 GPa

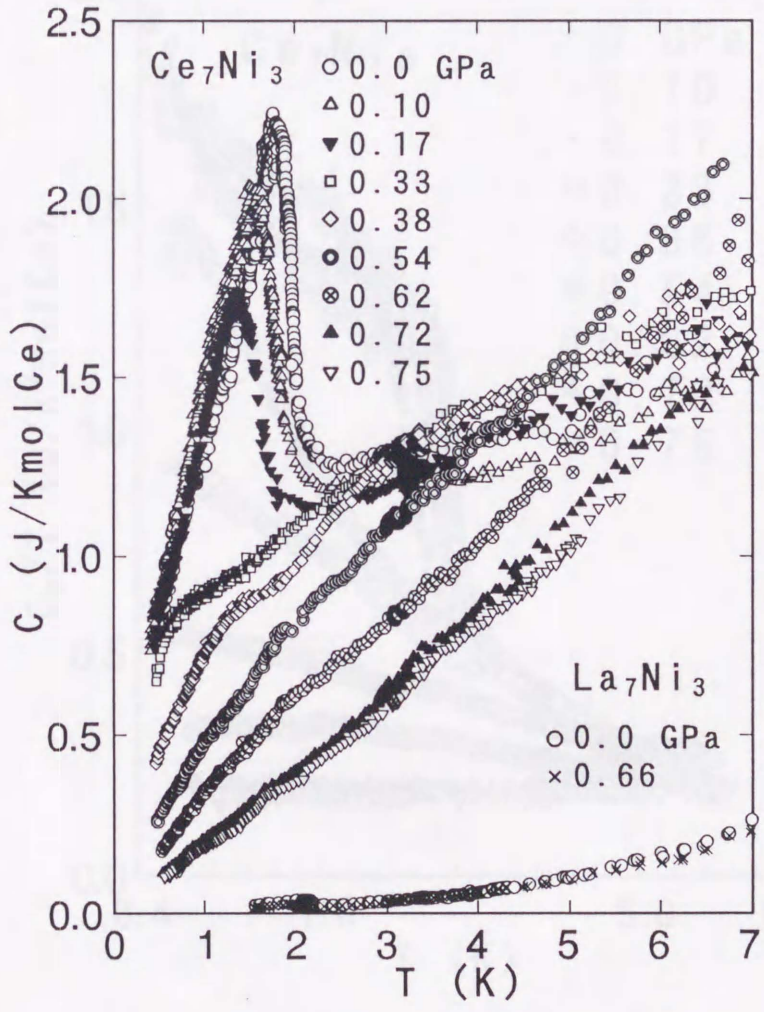

Fig. 17. Temperature dependence of the specific heat of Ce_7Ni_3 and La_7Ni_3 at various pressures.

and 0.69 GPa. Thus obtained C_m/T is plotted in Fig. 18 versus log$T$. At 0.33 GPa, the C_m/T curve shows an upturn. At 0.38 GPa, however, C_m/T is proportional to $-\log T$ over more than one decade in T, which is the NFL behavior. At a higher pressure 0.54 GPa, C_m/T has a downward curvature below 4 K. Above 0.62 GPa, C_m/T is saturated at low temperatures, indicating the recovery of the normal Fermi-liquid state. The variation of $\chi_{AC}(T)$ and $C(T)$ indicates that the crossover from non–Fermi–liquid behavior to normal Fermi-liquid behavior takes place between 0.38 and 0.62 GPa.

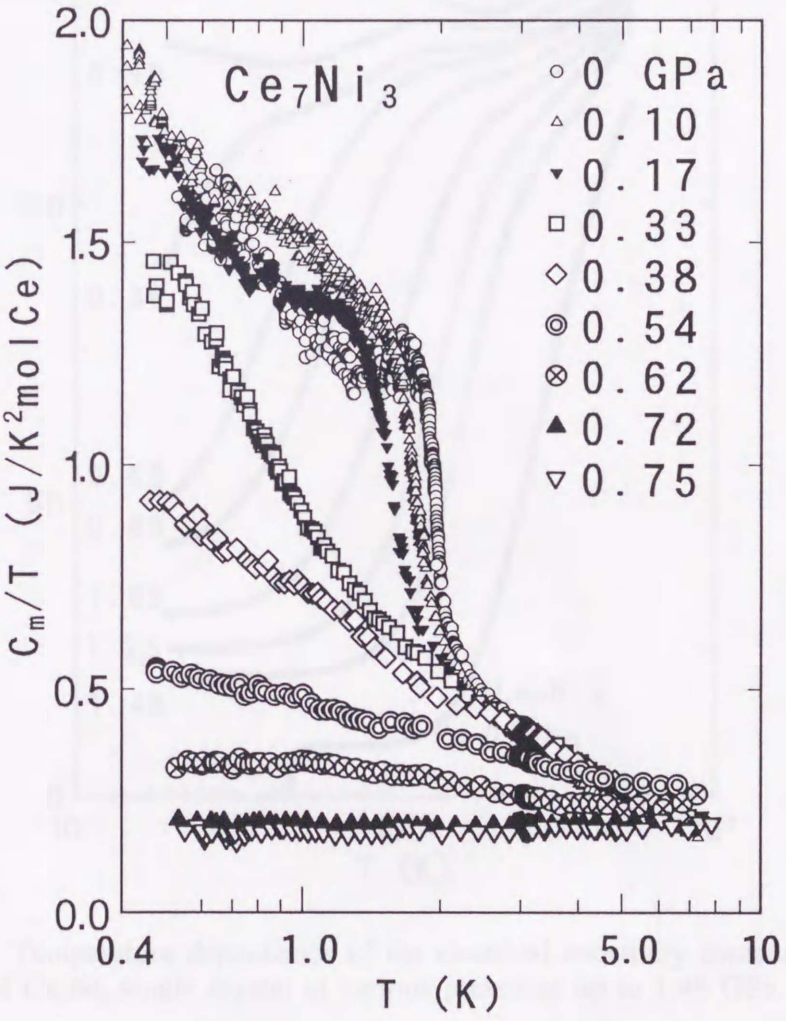

Fig. 18. Magnetic contribution to the specific heat C_m/T vs. log$T$ at various pressures.

3.2.4. Electrical resistivity

Figure 19 shows the temperature dependence of electrical resistivity $\rho(T)$ along the c axis of Ce_7Ni_3 single crystal at various pressures up to 1.48 GPa. With applying pressure, $\rho(T)$ strongly decreases over the temperature range, and eventually $\rho(T)$ approaches that of La_7Ni_3.

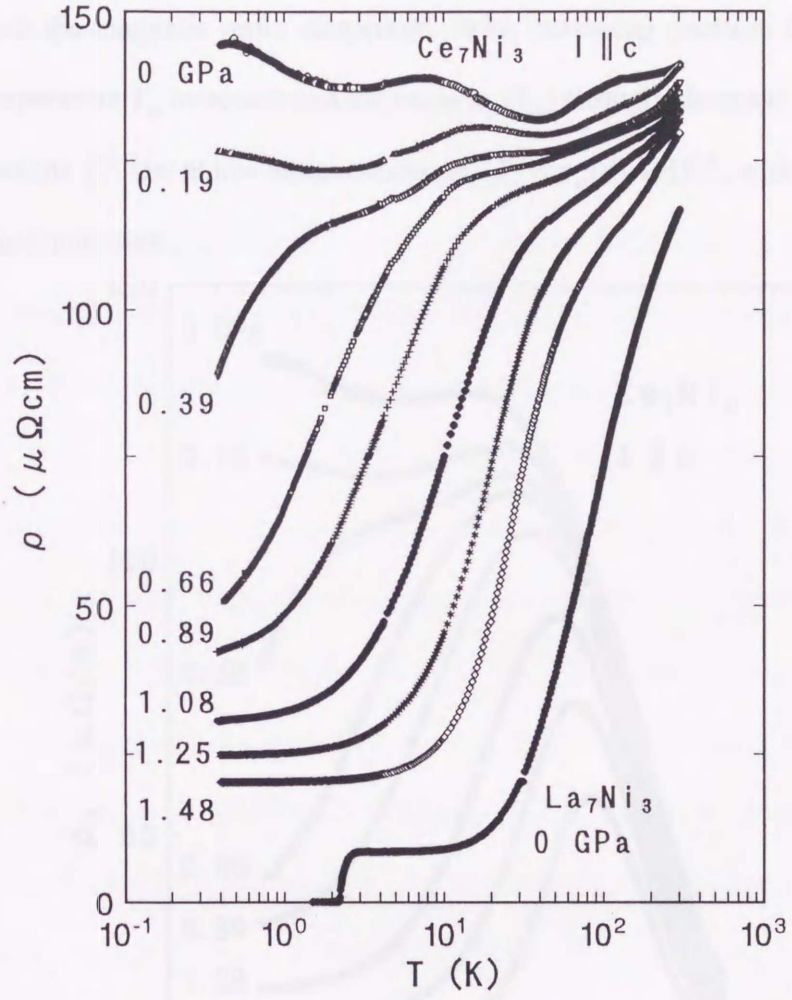

Fig. 19. Temperature dependence of the electrical resistivity measured along the c axis of Ce_7Ni_3 single crystal at various pressures up to 1.48 GPa.

The magnetic contribution to $\rho(T)$ from 4f electrons was estimated by using the same relation at ambient pressure, i.e., $\rho_m(P,T) = \rho(Ce_7Ni_3) - \rho(La_7Ni_3)$. As shown in Fig. 20, $\rho_m(T)$ in high temperature range is proportional to $-\log T$ with the almost unchanged slope over the whole pressure range. At ambient pressure, ρ_m exhibits two maxima at 8 K and 0.5 K and a local minimum around 2 K. The lower maximum at 0.5 K may be related with the anomaly at 0.6 K in M/H curve for $H \parallel b$. This maximum in ρ_m disappears above 0.33 GPa, at which the magnetic order disappears. With increasing pressure further, the higher maximal temperature T_m increases and the value $\rho_m(T_m)$ strongly decrease. Above 0.66 GPa, $\rho_m(T)$ follows the T^2 law at low temperatures, $\rho_m(T) = \rho_m(0) + AT^2$, which is characteristic of the Fermi-liquid state.

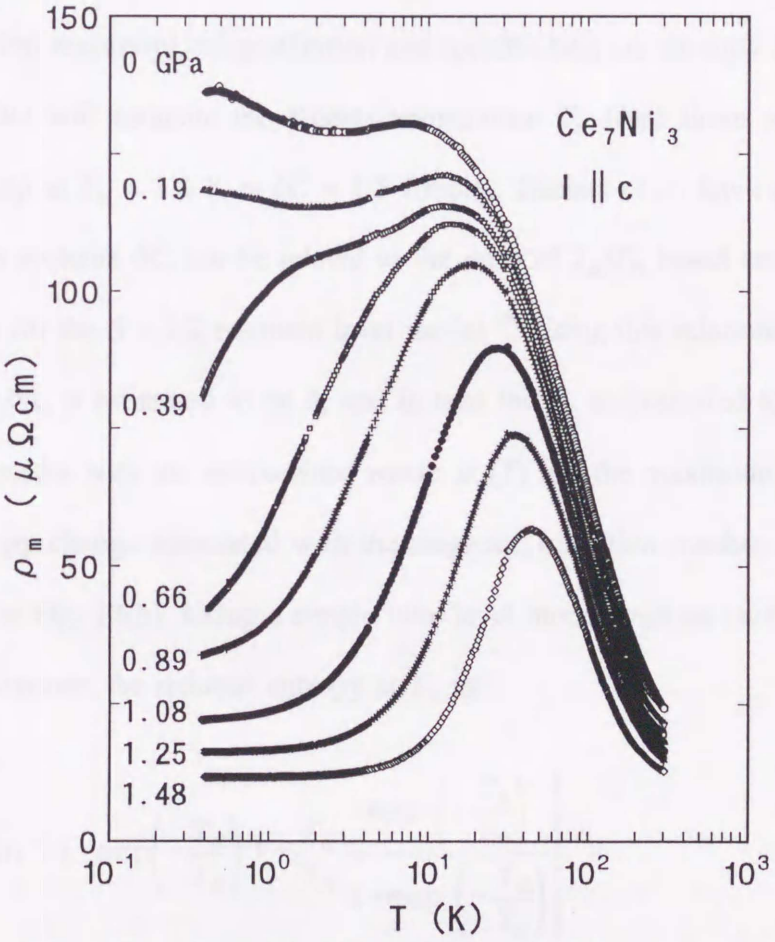

Fig. 20. Magnetic contribution to electrical resistivity ρ_m for Ce_7Ni_3 along the c axis vs. temperature at various pressures.

4. Discussion

4.1. Electronic state of Ce_7Ni_3 at ambient pressure

In this section, we discuss the valence and magnetic state of Ce_7Ni_3 at ambient pressure. The anisotropy in both the electrical resistivity and magnetic susceptibility is weak for the paramagnetic state, even though the compound has a hexagonal crystal structure. Strong anisotropy was found in the resistivity and magnetization curve below T_N. From L_{III}–XANES spectra and magnetic susceptibility measurements, the valence states of Ce ions in all the three sites are found to be very close to 3. Therefore, the electronic states of Ce ions in the Ce III site may not be distinguishable from those in the I and II sites.

The electrical resistivity, magnetization and specific heat are strongly affected by the Kondo effect. We will estimate the Kondo temperature T_K from these properties. The specific heat jump at T_N = 1.8 K is δC = 1.5 J/molK. Besnus et al. have shown that for many Ce Kondo systems δC can be related to the ratio of T_K/T_N based on the molecular field calculation for the S = 1/2 resonant level model.[39] Using this relationship, the value of T_K/T_N for Ce_7Ni_3 is estimated to be 3, and in turn the T_K is evaluated to be 6 K. This value of T_K coincides with the temperature where $\rho_m(T)$ has the maximum.

The entropy change associated with the magnetic transition reaches 47 % of Rln2 at T_N as shown in Fig. 13(b). Using a simple two–level model with an energy splitting of k_BT_K,[40] we can express the reduced entropy at T_N as

$$S_m = R\left[\ln\left\{1+\exp\left(-\frac{T_K}{T_N}\right)\right\}+\frac{T_K}{T_N}\frac{\exp\left(-\frac{T_K}{T_N}\right)}{1+\exp\left(-\frac{T_K}{T_N}\right)}\right]. \qquad (2)$$

By using the values of S_m =2.7 J/KmolCe for Ce_7Ni_3 at T_N, we obtain T_K = 4 K, which agrees with the value estimated by the δC. This T_K is within the values for typical heavy-fermion compounds such as $CeCu_6$ (5 K),[41] $CeAl_3$ (6 K)(ref. 41) and $CeCu_2Si_2$ (10 K).[42]

4.2. Pressure dependence of antiferromagnetic transition temperature

The pressure dependence of T_N of Ce_7Ni_3 determined from $\chi_{AC}(T)$ and $C(T)$ is shown in Fig. 21. Assuming the form $T_N \propto |P-P_c|^n$, the parameter P_c and n is estimated to be 0.32 GPa and 0.63, respectively, by the fit shown by the solid line in the figure. The exponent n for Ce_7Ni_3 is close to 2/3, which value was predicted for an antiferromagnet in three spatial dimension by Millis using renormalization-group techniques.[43] From the result of Fig.21, Grüneisen parameter $\Gamma_N = \partial \ln T_N / \partial \ln V$ at P = 0 is found to be 74. The value is

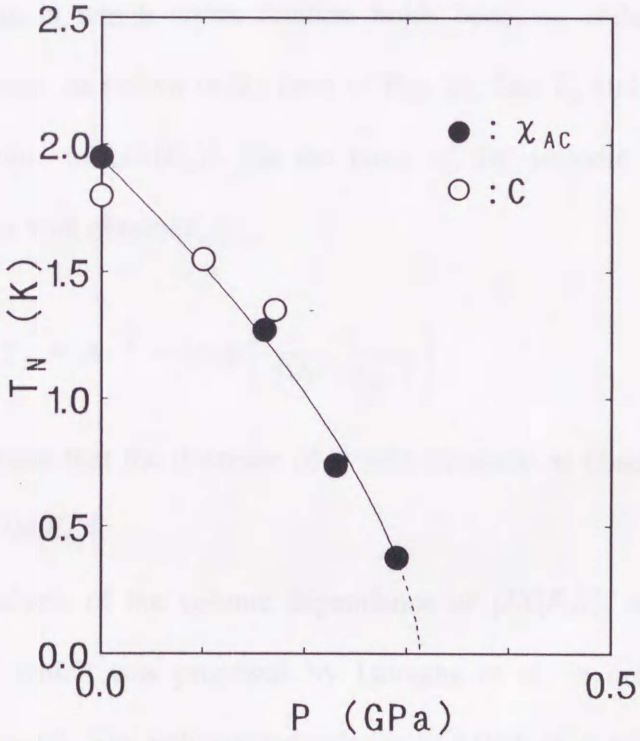

Fig. 21. Pressure dependence of T_N determined by AC magnetic susceptibility (●) and specific heat (○) measurements. The solid line shows the fitting curve by the form $T_N = C|P-P_c|^n$.

much greater than that of Ce compounds with similar values of T_N such as $CeAl_2$ (T_N = 3.8 K, Γ_N = 12).[14] The Γ_N for Ce_7Ni_3 becomes about 3000 around 0.3 GPa. The large Grüneisen parameter may be the combined effects of the electronic state being close to the magnetic–nonmagnetic transition and of the critical balance between the Kondo and RKKY interaction at ambient pressure.

4.3. Pressure dependence of Kondo temperature in the Fermi–liquid region

Let us discuss the pressure dependence of T_K estimated from the coefficient A of the T^2–dependence of electrical resistivity in the Fermi–liquid region above 0.66 GPa. For $P \geq 0.66$ GPa, from the double–logarithmic plot in Fig. 22, we find the relation $\rho_m(T) - \rho_m(0) = AT^2$ in the low–T range, as indicated by straight lines. As pressure increases, the temperature range in which above relation holds becomes wider and the coefficient A drastically decreases, as shown in the inset of Fig. 22. The T_K and the coefficient A can be related to the value of $|JN(E_F)|$. On the basis of the periodic Anderson model,[44] the following relation was obtained, i.e.,

$$T_K \propto A^{-\frac{1}{2}} \propto \exp\left(\frac{-1}{|JN(E_F)|}\right) . \qquad (4)$$

This equation means that the decrease of A with pressure as observed in Fig. 22 leads to the increase of $|JN(E_F)|$.

For the analysis of the volume dependence of $|JN(E_F)|$, we use the compressible Kondo model,[13] which was proposed by Lavagna et al. in order to explain the γ–α transition of Ce metal. The volume dependence of $|JN(E_F)|$ is assumed as follows,

$$|JN(E_F)| = |JN(E_F)|_0 \exp\left(-q\frac{V-V_0}{V_0}\right) , \qquad (5)$$

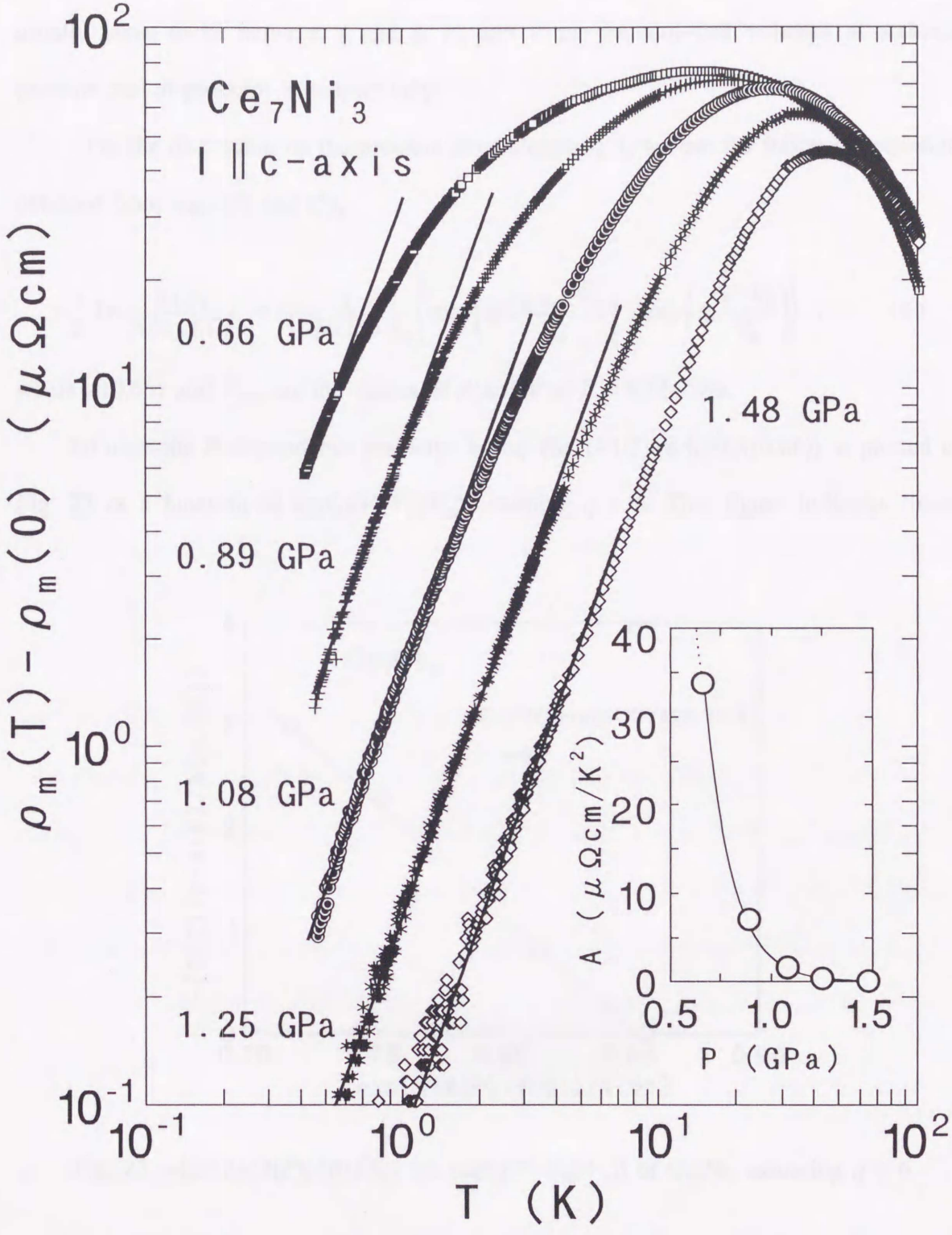

Fig. 22. Double-logarithmic plot of the magnetic contribution to electrical resistivity $\rho_m(T) - \rho_m(0)$ vs T for Ce_7Ni_3 at various pressures. Solid lines represent the form $\rho_m(T) - \rho_m(0) = AT^2$. The pressure dependence of A is shown in the inset.

where $|JN(E_F)|_0$ is the value of $|JN(E_F)|$ at ambient pressure, q is a numerical constant usually taken to be between 6 and 8, V_0 and V are the unit-cell volumes at ambient pressure and at pressure P, respectively.

For the discussion on the pressure dependence of A, we use the following equation obtained from eqs. (4) and (5),

$$-\frac{1}{2}\ln\frac{A(P)}{A(0.66)} = \frac{1}{|JN(E_F)|_0}\left\{\exp\left(q\frac{V_{0.66}-V_0}{V_0}\right)-\exp\left(q\frac{V-V_0}{V_0}\right)\right\} . \qquad (6)$$

where $A(0.66)$ and $V_{0.66}$ are the values of A and V at P = 0.66 GPa.

To trace the P-dependence predicted by eq. (6), $(-1/2)\ln(A(P)/A(0.66))$ is plotted in Fig. 23 as a function of $\exp(q(V-V_0)/V_0)$ assuming q = 6. This figure indicates linear

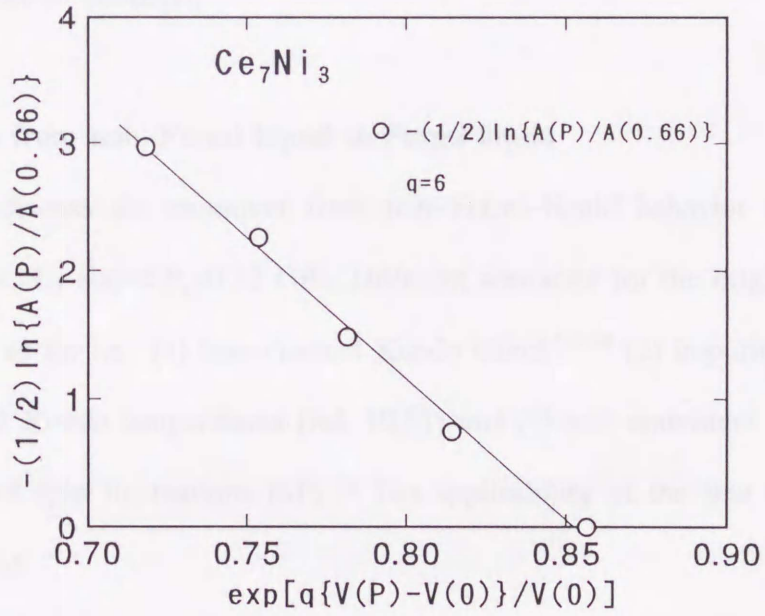

Fig. 23. $-(1/2)\ln(A(P)/A(0.66))$ vs. $\exp(q(V-V_0)/V_0)$ of Ce_7Ni_3 assuming q = 6.

dependence on the parameter $\exp(q(V-V_0)/V_0)$. The slope of $A(P)$ yields the values 4.5×10^{-2} for $|JN(E_F)|_0$. The value is about half those for typical heavy-fermion compounds $CeCu_6$ (9.1×10^{-2}) and $CeInCu_2$ (8.1×10^{-2})[45] estimated by the similar method. From eqs. (4) and (5), we obtain

$$\Gamma_e^* = \frac{1}{2}\frac{\partial lnA}{\partial lnV}$$

$$= \frac{q}{|JN(E_F)|_0}\left(\frac{V}{V_0}\right)\exp\left(q\frac{V-V_0}{V_0}\right) . \qquad (7)$$

Equation (7) indicates that the value of Γ_e^* is inversely proportional to $|JN(E_F)|_0$ and increases exponentially with volume. Assuming q = 6, $\Gamma_e^*(P$ = 0.66 GPa) is estimated to be 110. The critical value of $|JN(E_F)|_C$ for Ce_7Ni_3 is obtained to be $4.9\text{x}10^{-2}$ from eq. (5). The large values of Γ_e^* and Γ_N for Ce_7Ni_3 can be ascribed to the fact that the value of $|JN(E_F)|_0$ is close to $|JN(E_F)|_C$.

4.4. Crossover from non-Fermi liquid to Fermi liquid

We now discuss the crossover from non-Fermi-liquid behavior to Fermi liquid behavior for Ce_7Ni_3 above P_c=0.32 GPa. Different scenarios for the origin of NFL have been proposed so far i.e., (1) two-channel Kondo effect,[3-5,46] (2) impurity Kondo model with distributed Kondo temperatures (ref. 10,11) and (3) self-consistent renormalization (SCR) theory of spin fluctuations (SF).[12] The applicability of the first two models are briefly discussed.

4.4.1. Two-channel Kondo effect

Cox has shown that the two-channel magnetic Kondo effect arises in cerium compounds with Ce^{3+} ions which have a Γ_7 ground state in cubic symmetry sites (point

group O) or a Γ_9 ground state in hexagonal symmetry sites (point group D_6) site.[46]

Among the three nonequivalent Ce sites in Ce_7Ni_3, the site I for one Ce atom has trigonal symmetry (point group C_{3v}), and the sites II and III with three Ce atoms each have monoclinic symmetry (point group C_{1v}). It is unlikely that the two-channel magnetic Kondo effect arises from the 4f electrons in these symmetry sites.

4.4.2. Impurity Kondo model with distributed Kondo temperatures

Next, we will discuss the applicability of the impurity Kondo model with distributed Kondo temperatures. Because there are nonequivalent sites for Ce atoms in Ce_7Ni_3, the exchange coupling between the 4f and conduction electrons J may distribute so that the T_K may be different for the three sites. In general, T_K may depend on the site symmetry and inter-atomic spaces of Ce ions. Considering the Ce and Ni atoms as rigid spheres, atomic radii of Ce_I, Ce_{II}, and Ce_{III} are estimated to be 1.81 Å, 1.76 Å, and 1.72 Å, respectively.[20] Therefore, we assume that the Kondo temperatures are in order of the inverse of the volume, $T_{K1}(Ce_I) < T_{K2}(Ce_{II}) < T_{K3}(Ce_{III})$. We further assume that the magnetic specific heat C_m is described by the summation of independent contributions from three types of Kondo impurities with spin 1/2, $C_m/T = C_{K1}(I) + C_{K2}(II) + C_{K3}(III)$. The fitted results of $C_{K1} + C_{K2} + C_{K3}$ for 0.38 GPa and 0.54 GPa are shown by dotted lines in Figs. 24(a) and 24(b). T_{K1}, T_{K2} and T_{K3} are respectively 2, 10 and 24 K at 0.38 GPa, and 5.5, 19 and 30 K at 0.54 GPa. For comparison, the results of SCR theory(C_{SCR}) are shown in the solid lines. We will see that the SCR theory with less fitting parameters reproduce better the experimental data than the impurity Kondo model.

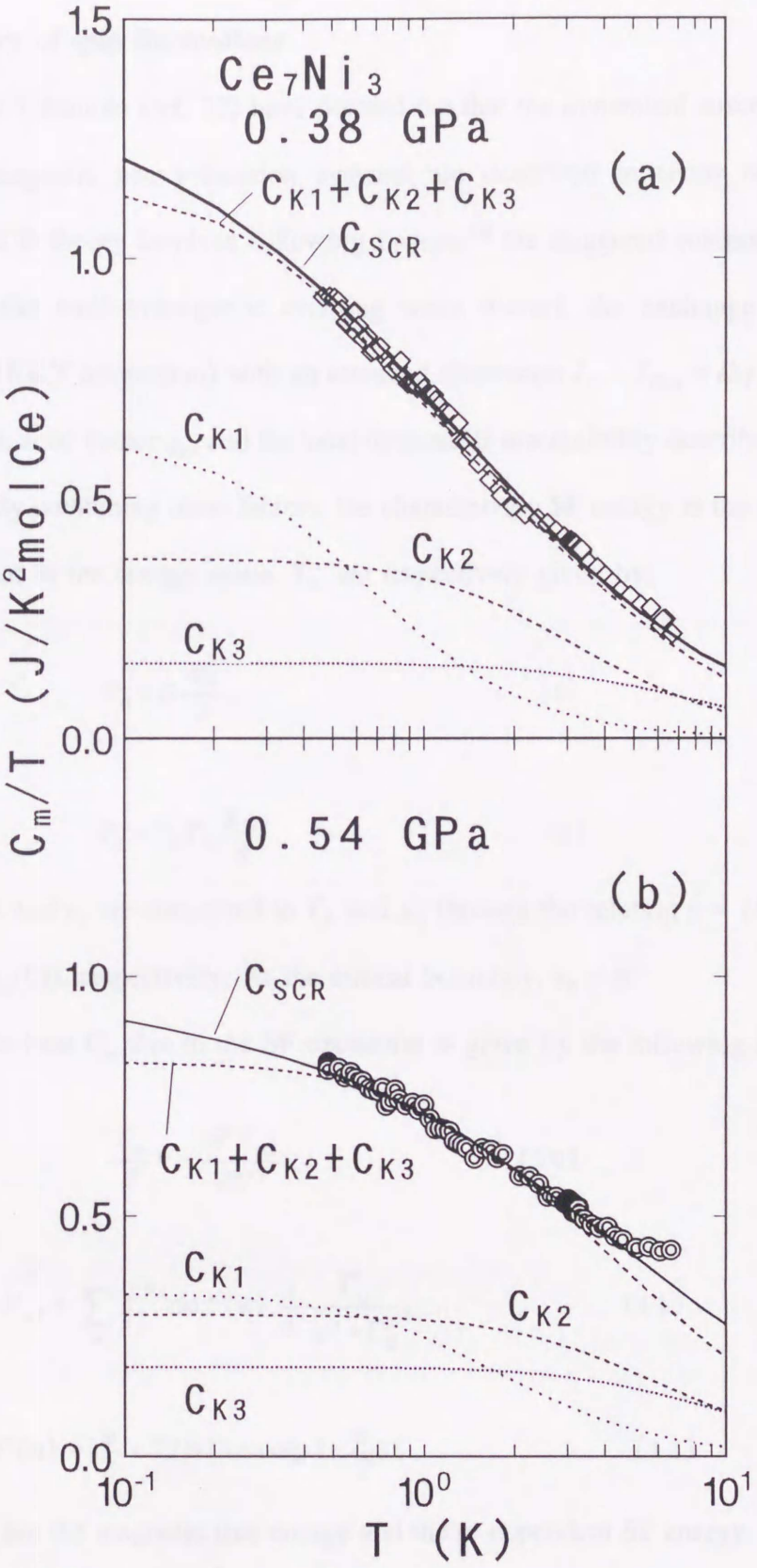

Fig. 24. Magnetic specific heat C_m/T at 0.38 GPa (a) and 0.54 GPa (b) fitted with the impurity Kondo model with three Kondo temperatures for the three Ce sites. The solid lines, C_{SCR}, represent the fits by the SCR theory.

4.4.3. SCR theory of spin fluctuations

Moriya and Takimoto (ref. 12) have pointed out that the dynamical susceptibility of nearly antiferromagnetic heavy-fermion systems are described in terms of the SCR equations. The SCR theory involves following factors;[12] the staggered susceptibility at 0 K, $\chi_Q(0)$ (Q is the antiferromagnetic ordering wave vector), the exchange energy J_Q (roughly of the RKKY interaction) with an assumed dispersion $J_Q - J_{Q+q} = Dq^2$ up to the effective Brillouin zone vector q_B, and the local dynamical susceptibility described as $\chi_L(\omega) = \chi_L/(1-i\omega/\Gamma_L)$. By combining these factors, the characteristic SF energy in the momentum space, T_A, and that in the energy space, T_0, are respectively given by,

$$T_A = D\frac{q_B^2}{2}, \qquad (8)$$

$$T_0 = T_A\Gamma_L\frac{\chi_{L0}}{\pi}. \qquad (9)$$

The parameters y and y_0 are connected to T_A and χ_Q through the relation $y = 1/(2T_A\chi_Q(T))$ and $y_0 = 1/(2T_A\chi_Q(0))$, respectively. At the critical boundary, $y_0 = 0$.

The specific heat C_m due to the SF excitation is given by the following expression:

$$\frac{C_m}{T} = -\frac{\partial^2 F_{sf}}{\partial T^2}, \qquad (10)$$

$$F_{sf} = \sum_q \int_0^{\omega_c} d\omega f(\omega)\frac{3}{\pi}\frac{\Gamma_q}{\omega^2+\Gamma_q^2}, \qquad (11)$$

$$f(\omega) = \frac{\omega}{2} + T\ln[1-\exp(-\frac{\omega}{T})]. \qquad (12)$$

where F_{sf} and Γ_q are the magnetic free energy and the q-dependent SF energy. Neglecting the contribution from zero-point fluctuations, C_m at very low temperature is given by:

$$\frac{C_m}{T} = \frac{3R}{2}\frac{1}{T_0}\left[\chi_c - \frac{\pi}{2} y^{\frac{1}{2}}\right] . \qquad (13)$$

where χ_c is the cut-off wave vector in units of q_B. In Fig. 25(a), C_m divided by the reduced temperature $t = T/T_0$ is shown versus log$t$. At the magnetic instability, $y_0 = 0$, C_m/T in the low T limit is finite and decreases in proportion to $T^{1/2}$, and then shows the log$T$ dependence in the temperature range $T \sim T_0$.

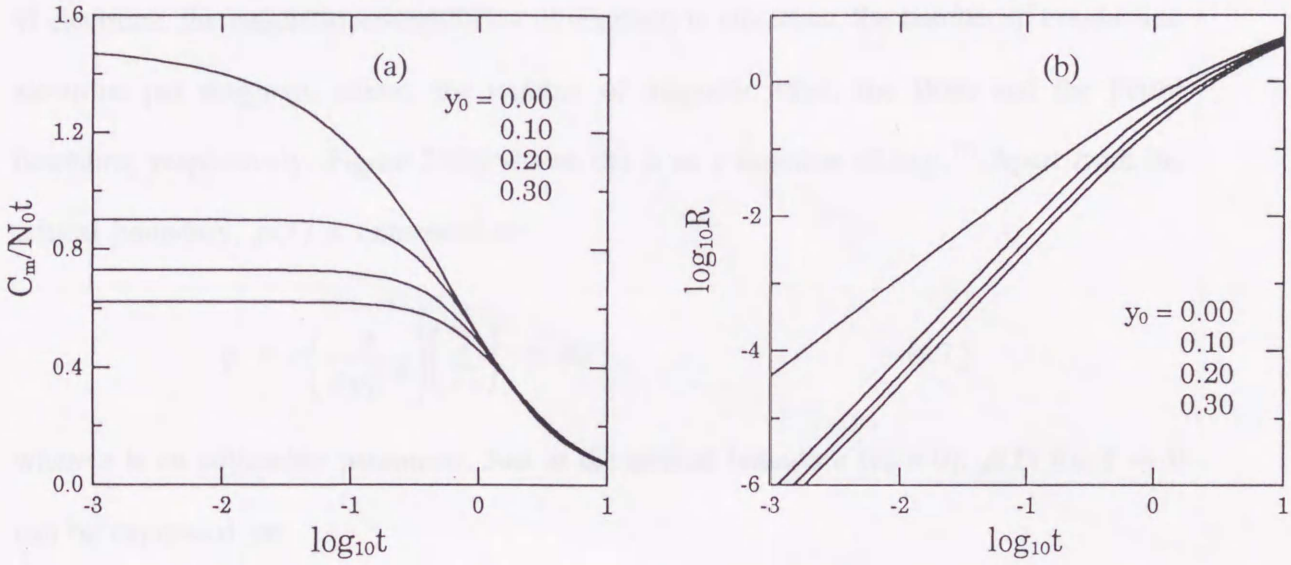

Fig. 25. (a)Specific heat divided by reduced temperature $t = T/T_0$ calculated by the SCR theory just at ($y_0 = 0$) and around ($y_0 > 0$) the antiferromagnetic instability. (b)Temperature dependence of electrical resistivity calculated by the SCR theory just at ($y_0 = 0$) and around ($y_0 > 0$) the antiferromagnetic instability (from ref. 12).

The static uniform susceptibility χ_n at $T \approx 0$ K can be expressed as:

$$\frac{1}{\chi_n} = 2(1+y_0)\,T_A. \qquad (14)$$

The electrical resistivity ρ is given by:

$$\rho = \frac{6\hbar J_K}{e^2 n^2 \pi T N_0^2} \sum_q q_x^2 \int_{-\infty}^{\infty} d\omega\, n(\omega)\,[n(\omega)+1]\,\chi_c''(q,\omega)\,Im\chi(q,\omega) \qquad (15)$$

$$N_0 \chi_c''(q,\omega) = \pi \sum_k \delta(\epsilon_k - \epsilon_{k-q} - \omega)\,[f(\epsilon_{k-q}) - f(\epsilon_k)], \qquad (16)$$

where J_K, χ_c'', n_c, N_0, $n(\omega)$ and $f(\varepsilon)$ are the exchange coupling between the conduction and 4f electrons, the magnetic susceptibility of conduction electrons, the number of conduction electrons per magnetic atoms, the number of magnetic sites, the Bose and the Fermi functions, respectively. Figure 25(b) shows the ρ as a function of log$t$.[12] Apart from the critical boundary, $\rho(T)$ is expressed as:

$$\rho = r\left(\frac{\pi}{8y_0^{0.5}}\right)\left(\frac{T}{T_0}\right)^2 = AT^2, \qquad (17)$$

where r is an adjustable parameter. Just at the critical boundary ($y_0 = 0$), $\rho(T)$ for $T \rightarrow 0$ can be expressed as:

$$\rho(T) \propto \left(\frac{T}{T_0}\right)^{\frac{3}{2}}. \qquad (18)$$

In the temperature region $T \sim T_0$, ρ is proportional to t.

4.4.4. Application of SCR theory to Ce_7Ni_3 near the antiferromagnetic instability

We now apply the SCR theory to describe the observed $C_m(T)$, $\chi_{AC}(T)$ and $\rho_m(T)$ of Ce_7Ni_3 by using three parameters y_0, χ_c and T_0,[12] where we assume that the electronic states

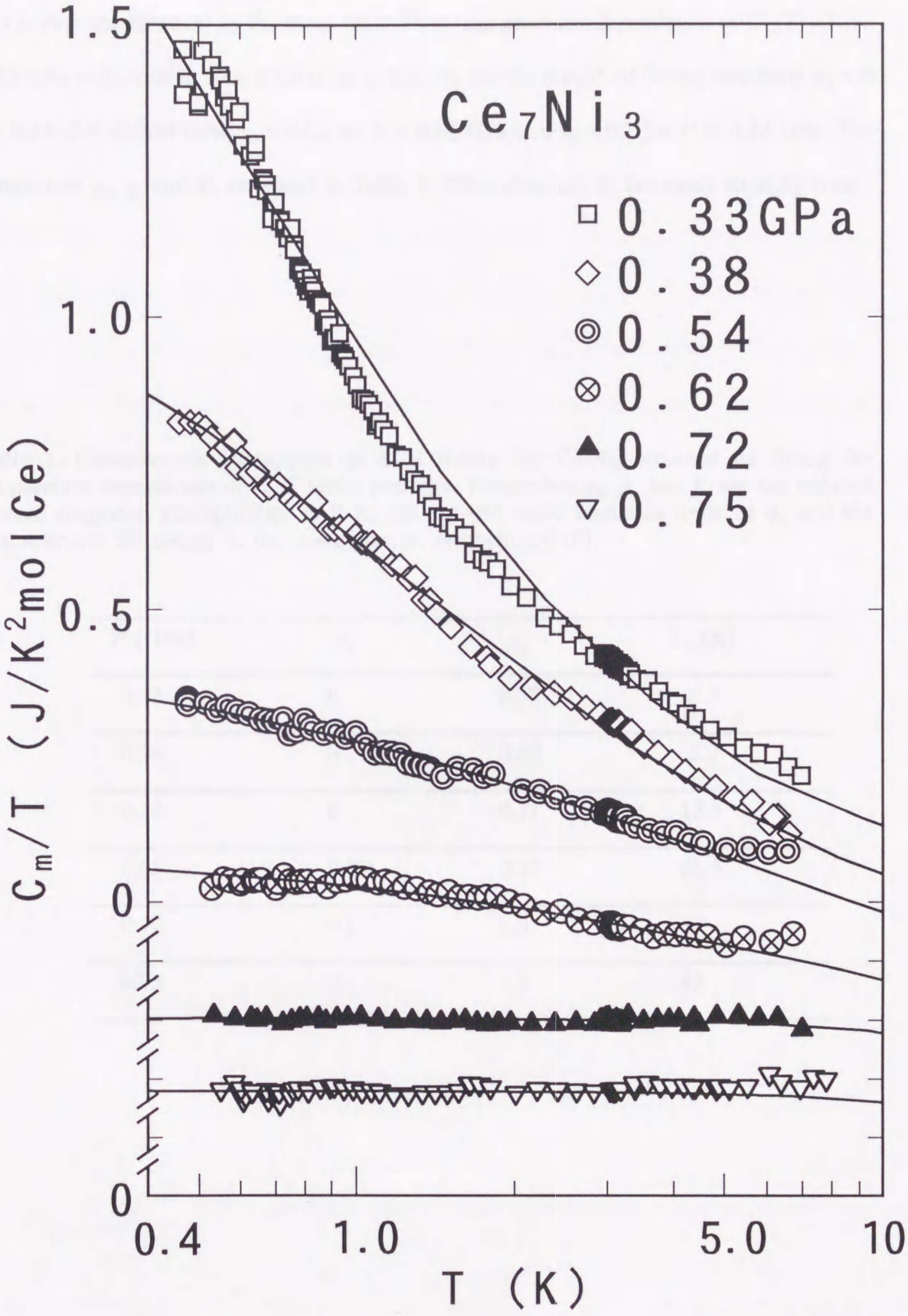

Fig. 26. Magnetic specific heat divided by temperature C_m/T vs. log$T$ above 0.33 GPa. Solid lines indicate the fit with the SCR theory (see text). Data for each P are shifted downward consecutively by 0.1 J/K^{2}molCe for clarity.

of Ce ions are identical in the three sites. First, the pressure dependence of $C_m(T)$ above 0.33 GPa is discussed. The solid lines in Fig. 26 are the results of fitting assuming $y_0 = 0$ for $0.33 \leq P \leq 0.54$ GPa, $y_0 = 0.02$ for $P = 0.62$ GPa and $y_0 = 0.1$ for $P \geq 0.72$ GPa. The parameters y_0, χ_c and T_0 are listed in Table 1. Thus obtained T_0 increases strongly with

Table 1. Characteristic parameters of SCR theory for Ce_7Ni_3 obtained by fitting the temperature dependence of C_m/T under pressure. Parameters y_0, χ_c and T_0 are the reduced inverse staggered susceptibility at 0 K, the cut-off wave vector in units of q_B and the characteristic SF energy in the energy space, respectively[10].

P (GPa)	y_0	χ_c	T_0 (K)
0.33	0	0.57	2.3
0.38	0	0.60	5.2
0.54	0	0.71	13.5
0.62	0.02	0.75	21.5
0.72	0.1	1.0	37
0.75	0.1	1.0	42

pressure as shown in Fig. 27. At the critical boundary, C_m/T is expected to follow the form $C_m/T = \gamma_0 - \beta T^{1/2}$ for $T \ll T_0$. This form is not observed at P = 0.33 and 0.38 GPa down to 0.5 K because this temperature is not sufficiently below T_0. At P = 0.54 GPa, however, C_m/T follows the above form between 0.5 and 3 K, being far below T_0 = 13.5 K. The Grüneisen parameter $\Gamma_e = -\partial \ln T_0/\partial \ln V$ is estimated to be 220 around 0.4 GPa using the bulk modulus B_0 = 24.6 GPa. The value of Γ_e for Ce_7Ni_3 decreases with increasing pressure and becomes 110 around 0.7 GPa. For other systems showing NFL behavior such as $Ce_{1-x}La_xRu_2Si_2$ and $CeCu_{6-x}Au_x$, T_0 hardly changes near the critical boundary when the unit-cell volume is decreased by decreasing x.[47,48]

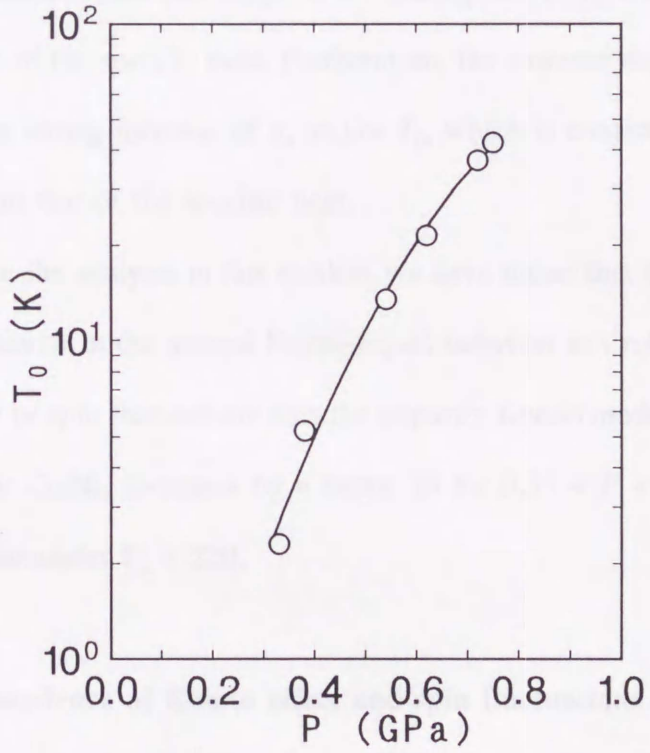

Fig. 27. Pressure dependence of the characteristic temperature of spin fluctuations T_0 for Ce_7Ni_3.

It is noteworthy that the value of χ_{AC} at 0.6 K in Fig.16 is reduced by one order of magnitude in the measured pressure range. From eq. (14), the observed decrease of χ_{AC} implies the increase of y_0 and/or T_A with increasing pressure. The relation of $J_Q/T_A = 1$ (ref. 12) in turn suggests that pressure increases the RKKY interaction energy J_Q.

As mentioned previously, SCR theory predicts $\rho(T) \propto (T/T_0)^{3/2}$ near the critical pressure. However, at P = 0.39 GPa, $\rho_m(T)$ in the low–T range can not be described by the power law because our temperature range is not sufficiently low compared to T_0 = 5.2 K. For $P \geq 0.66$ GPa, from in Fig. 22, we find the relation $\rho_m(T) - \rho_m(0) = AT^2$ in the low–T range, as indicated by straight lines. As shown in the inset of Fig. 22, the value A seems to diverge below 0.66 GPa, which tendency is expected from eq. (17) when the critical boundary is approached. This fact supports the assumption of $y_0 = 0$ below 0.54 GPa for the above analysis of the specific heat. Furthermore, the extreme depression of A for $P \geq$ 0.66 GPa indicates strong increase of y_0 and/or T_0, which is consistent with the result of $T_0(P)$ deduced from that of the specific heat.

To summarize the analysis in this section, we have found that the crossover in $C_m(T)$ from the NFL behavior to the normal Fermi–liquid behavior in Ce_7Ni_3 is better described by the SCR theory of spin fluctuations than the impurity Kondo model. It is also found that the value of T_0 for Ce_7Ni_3 increases by a factor 20 for $0.33 < P < 0.75$ GPa, yielding a large Grüneisen parameter $\Gamma_e = 220$.

4.5. Pressure dependence of Kondo effect and spin fluctuations

In this section, we discuss the pressure dependence of specific heat and electrical resistivity in the normal Fermi–liquid region above 0.62 GPa. In the Fermi–liquid state, the Sommerfeld coefficient, γ, and the coefficient A of the T^2–dependence of electrical

resistivity are related by $\gamma^2 \propto A$. For many Ce- and U-based compounds, A/γ^2 has a universal value of 1.0×10^{-5} ($\mu\Omega$cm/K^2)/(mJ/molK^2).[49] The values of A at 0.62 and 0.75 GPa for Ce_7Ni_3 were estimated by the interpolation of the results of the inset of Fig. 22.

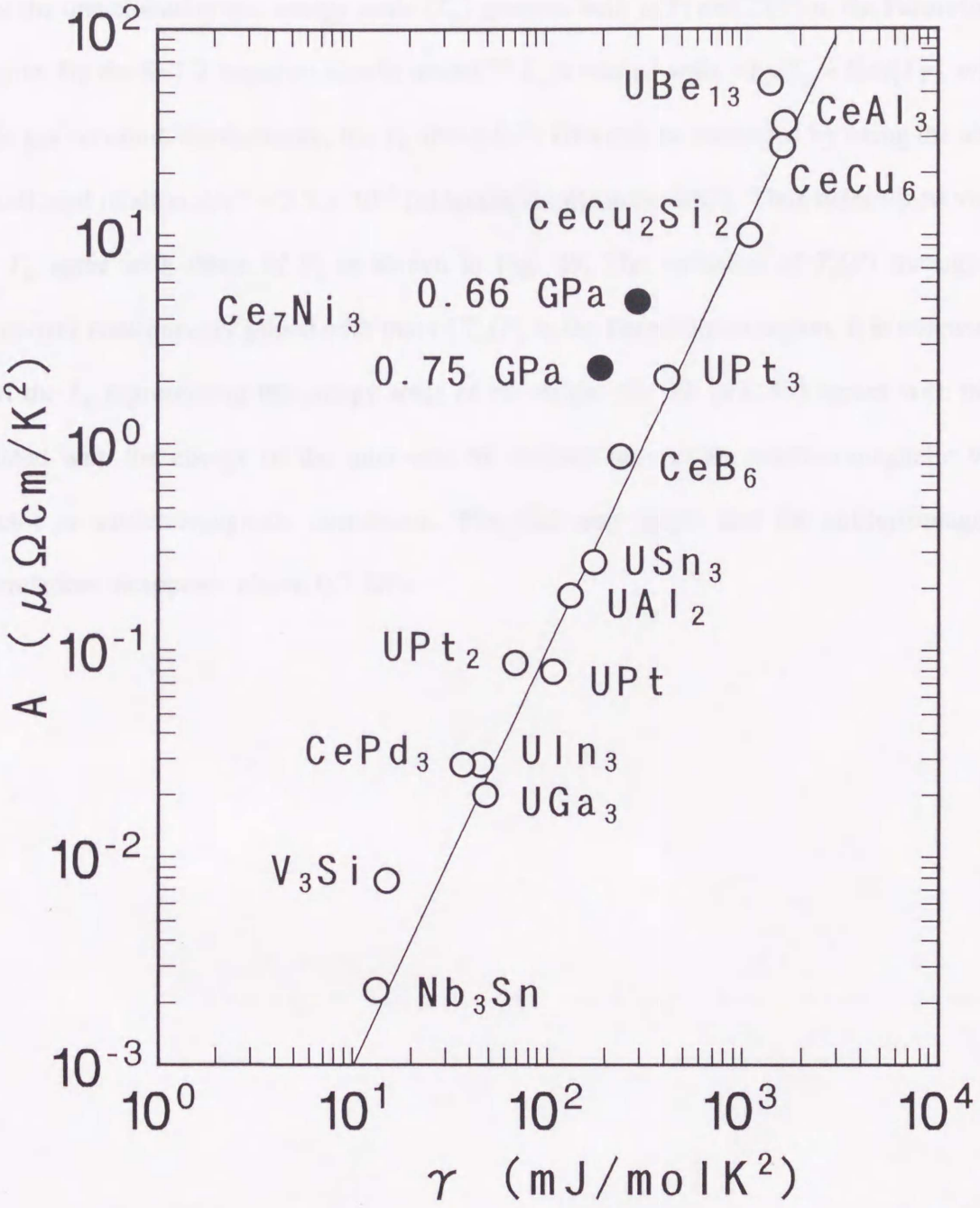

Fig. 28. Coefficient A of the T^2 term of the resistivity vs. the coefficient γ of the T-liner term of the specific heat for various compounds. The solid line represents the ratio of $A/\gamma = 1.0 \times 10^{-5}$ ($\mu\Omega$cm/K^2)/(mJ/molK^2).

In Fig. 28, A and γ for Ce_7Ni_3 are plotted on the data of some Ce– and U–based compounds. The value A/γ^2 at 0.62 and 0.75 GPa are 5.5×10^{-5} and 6.5×10^{-5} ($\mu\Omega$cm/K^2/mol)/(mJ/molK^2), respectively. These values are independent of pressure, which implies that the one characteristic energy scale (T_K) governs both $\rho(T)$ and $C(T)$ in the Fermi-liquid region. By the S=1/2 impurity Kondo model,[50] T_K is related with γ by $T_K = R\pi/(3\gamma)$, where R is gas constant. Furthermore, the T_K above 0.75 GPa can be estimated by using the above mentioned relation $A/\gamma^2 = 5.5 \times 10^{-5}$ ($\mu\Omega$cm/K^2/mol)/(mJ/molK^2). Thus determined values of T_K agree with those of T_0 as shown in Fig. 29. The variation of $T_0(P)$ through the crossover continuously joined with that of $T_K(P)$ in the Fermi-liquid region. It is noteworthy that the T_K representing the energy scale of the single–site SF (ref. 49) agrees with the T_0 related with the energy of the inter–site SF defined around the antiferromagnetic wave vector or antiferromagnetic correlation. This fact may imply that the antiferromagnetic correlation disappears above 0.7 GPa.

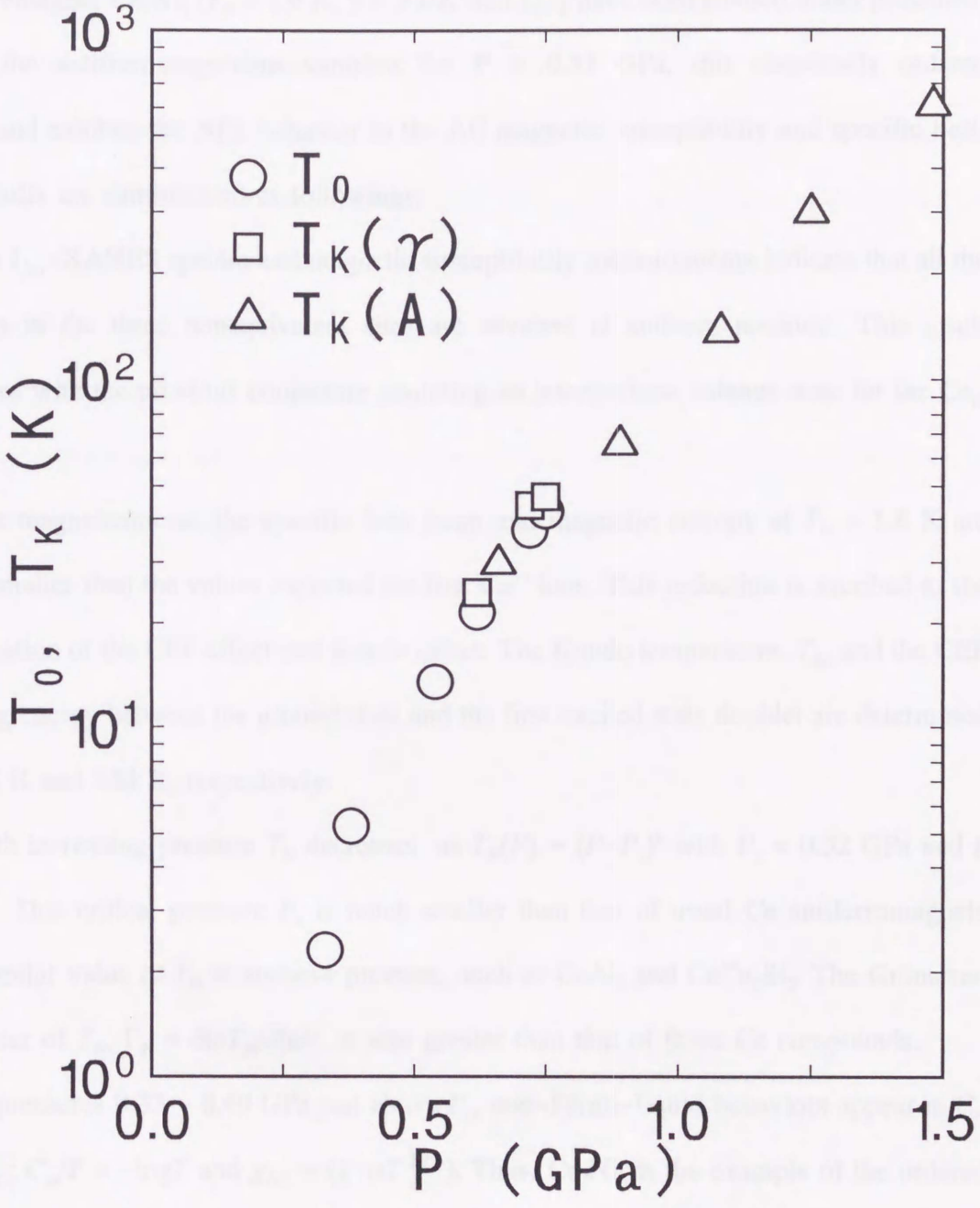

Fig. 29. Pressure dependence of the spin fluctuation temperature T_0 and Kondo temperature T_K for Ce_7Ni_3.

5. Conclusion

In this thesis, the transport, magnetic and thermal properties of the heavy-fermion antiferromagnet Ce_7Ni_3 (T_N = 1.9 K, γ = 9 J/K^{2}mol f.u.) have been studied under pressures. When the antiferromagnetism vanishes for $P \geq 0.33$ GPa, this chemically ordered compound exhibits the NFL behavior in the AC magnetic susceptibility and specific heat. The results are summarized as followings.

(1) The L_{III}-XANES spectra and magnetic susceptibility measurements indicate that all the Ce ions in the three nonequivalent sites are trivalent at ambient pressure. This result disagrees with the previous conjecture assuming an intermediate valence state for the Ce_{III} site.[19)]

(2) The magnetizations, the specific heat jump and magnetic entropy at T_N = 1.8 K are much smaller than the values expected for free Ce^{3+} ions. This reduction is ascribed to the combination of the CEF effect and Kondo effect. The Kondo temperature, T_K, and the CEF splitting energy between the ground state and the first excited state doublet are determined to be 5 K and 240 K, respectively.

(3) With increasing pressure T_N decreases as $T_N(P) \propto (P-P_c)^n$ with P_c = 0.32 GPa and n = 0.63. This critical pressure P_c is much smaller than that of usual Ce antiferromagnets with similar value of T_N at ambient pressure, such as $CeAl_2$ and $CeCu_2Si_2$. The Grüneisen parameter of T_N, $\Gamma_N = \partial \ln T_N / \partial \ln V$, is also greater than that of these Ce compounds.

(4) At pressures 0.33 ~ 0.49 GPa just above P_c, non-Fermi-liquid behaviors appear in C_m and χ_{AC}; $C_m/T \propto -\log T$ and $\chi_{AC} \propto (1-\alpha T^{1/2})$. Thus, Ce_7Ni_3 is the example of the ordered compound which shows NFL behavior near the magnetic instability. For P > 0.62 GPa, the normal Fermi-liquid behavior recovers, as indicated by $\rho(T) = \rho_0 + AT^2$, χ_{AC} = const., and C_m/T = const. at low temperatures.

(5) The Grüneisen parameter Γ_e^* of the Kondo temperature T_K estimated from the coefficient A of T^2-dependence of electrical resistivity above 0.66 GPa is evaluated to be 110 around 0.66 GPa. The large values of Γ_N and Γ_e^* for Ce_7Ni_3 can be ascribed to the fact that the value of $|JN(E_F)|_0$ is close to $|JN(E_F)|_C$.

(6) The crossover in $C_m(T)$ from the NFL behavior to the Fermi-liquid behavior is describable by the SCR theory of spin fluctuations. The characteristic spin-fluctuation energy T_0 increases by a factor of 20 for $0.32 \leq P \leq 0.75$ GPa, yielding a large Grüneisen parameter $\Gamma_e = 220$.

(7) The coefficient A and γ decrease strongly with increasing pressure above 0.62 GPa. The continuous increase in $T_0(P)$ through the crossover ($0.33 \leq P \leq 0.75$ GPa) joins with that of $T_K(P)$ in the Fermi-liquid region ($0.66 \leq P \leq 1.48$ GPa).

Acknowledgments

The author wishes to express his sincere thanks to Professor Toshiro Takabatake for numerous discussions and helpful suggestions. He also would like to thank Professor T. Moriya for the valuable discussions on the SCR theory and NFL behavior. He is very grateful to Emeritus Professor H. Fujiwara and Professors M. Nomura and H. Kadomatsu for their encouragement and valuable advice on the high pressure measurements. He thanks to Professor F. Iga, Dr. K. Katoh and Dr. H. Yamamoto for their discussions on the physical properties of Ce_7Ni_3 at ambient pressure. He also thanks K. Ishii, M. Kitagawa, M. Hayashi, S. Nishikawa, K. Imamoto, Y. Nishiyama, and H. Chono for their technical supports. He is thankful to Mr. K. Izawa, Dr. T. Suzuki and Professor T. Fujita, Department of Physics, Hiroshima University for their help in the measurement of specific heat at ambient pressure for Ce_7Ni_3 and La_7Ni_3 and helpful discussions. He is also grateful to Professor T. Komatsubara and Dr. N. Sato, Department of Physics, Tohoku University for the magnetization measurements below 1.5K.

Finally, the author would like to thank his late father and his mother and his friends for their encouragement.

References

1) S. Doniach, in: Valence Instability and Related Narrow-Band Phenomena, edited by R. D. Parks (Plenum Press, New York, 1977), p. 169.

2) N. Grewe and F. Steglich: Handbook on the Physics and Chemistry of Rare Earths, ed. K. A. Gschneidner, Jr. and L. Eyring (Elsevier, Amsterdam, 1991) Vol. 14, p. 343.

3) C. L. Seaman, M. B. Maple, B. W. Lee, S. Ghamaty, M. S. Torikachvili, J. -S. Kang, L. Z. Liu, J. W. Allen and D. L. Cox: Phys. Rev. Lett., **67**, 2882(1991).

4) H. Amitsuka, T. Hidano, T. Honma, H. Mitamura and T. Sakakibara: Physica B**186-188**, 337(1993).

5) F. G. Aliev, H. El Mfarrej, S. Vieira and R. Villar: Solid State Commun., **91**, 775(1994).

6) H. v. Löhneysen, T. Pietrus, G. Portisch, H. G. Schlager, A. Schröder, M. Sieck and T. Trappmann: Phys. Rev. Lett., **72**, 3262(1994).

7) F. Steglich, C. Geibel, K. Gloos, G. Olesch, C. Schank, C. Wassilew, A. Loidl, A. Krimmel and G. R. Stewart: J. Low Temp. Phys., **95**, 3(1994).

8) S. Kambe, S. Raymond, H. Suderow, J. Mc Donough, B. Fak, L. P. Regnault, J. Flouquet: Physica B, in press.

9) S. Kambe, S. Raymond, J. McDonough, L. P. Regnault, J. Flouquet, P. Lejay and P. Haen: J. phys. Soc. Jpn. in press.

10) V. Dobrosavljević, T. R. Kirkpatrick and G. Kotliar: Phys. Rev. Lett., **69**, 1113(1992).

11) O. O. Bernal, D. E. MacLaughlin, H. G. Lukefahr and B. Andraka: Phys. Rev. Lett., **75**, 2023(1995).

12) T. Moriya and T. Takimoto: J. Phys. Soc. Jpn., **64**, 960(1995).

13) M. Lavagna, C. Lacroix and M. Cyrot: Phys. Lett., A**90**, 210(1982).

14) P. Morin, C. Vettier, J. Flouquet, M. Konczykowski, Y. Lassailly, J.-M. Mignot,

U. Welp: J. Low Temp. Phys., **70**, 377(1988).

15) J. D. Thompson, R. D. Parks and H. Borges: J. Magn. Magn. Mater. **54–57**, 377(1986).

16) D. Jaccard, K. Behnia and J. Sierro: Phys. Lett., **A163**, 475(1992).

17) B. Bogenberger, H. v. Löhneysen: Phys. Rev. Lett., **74**, 1016(1995).

18) D. Gignoux and J. C. Gomez–Sal: J. Appl. Phys., **57**, 3125(1985).

19) J. G. Sereni, O. Trovarelli, J. P. Kappler, C. Paschke, T. Trappmann, and H. v. Löhneysen: Physica B**199–200**, 567(1994).

20) R. B. Roof, Jr., A. C. Larson and D. T. Cromer: Acta Cryst., **14**, 1084(1961).

21) R. A. Neifeld, M. Croft, T. Mihalisin, C. U. Segre, M. Madigan, M. S. Torikachvili, M. B. Maple, L. E. DeLong: Phys. Rev., B**32**, 6928(1985).

22) J. C. Fuggle, F. U. Hillebrecht, Z. Zolnierek, R. Lasser, Ch. Freiburg, O. Gunnarsson, and K. Schönhammer: Phys. Rev. B**27**, 7330(1983).

23) F. U. Hillebrecht, J. C. Fuggle, G. A. Sawatzky, M. Campagna, O. Gunnarsson, and K. Schönhammer: Phys. Rev. B**30**, 1777(1983).

24) K. A. Gschneider and M. E. Verkade: Document IS–RIC–7, 28–29(1974).

25) K. Gschneider, Jr., R. O. Elliott and R. R. McDonald: J. Phys. Chem. Solids, 23,555(1962).

26) G. L. Olcese: J. Less–Common Metals, 33, 71(1973).

27) H. Fujiwara, H. Kadomatsu and K. Tohma: Rev. Sci. Instrum., **51**, 1345(1980).

28) C. M. Brodbeck, R. R. Bukrey, and J. T. Hoeksema: Rev. Sci. Instrum., **49**, 1279(1978).

29) G. J. Piermarini, S. Block, J. D. Barnett, and R. A. Forman: J. Appl. Phys., 46, 2774(1975).

30) A. Eichler and W. Gey: Rev. Sci. Instrum., **50**, 1445(1979).

31) R. I. Boughton, J. L. Olsen and C. Palmy: Progress in Low Temp. Phys., vol. **6**, ed. C. J. Gortoer (North–Holland, Amsterdam, 1970) p. 163.

32) H. R. ÓNeal and N. E. Phillips: Phys. Rev. A**137**, 748(1965).

33) D. Wohlleben and J. Röhler: J. Appl. Phys., **55**, 1904(1984).

34) J. F. Herbst and J. W. Wilkins: Phys. Rev. B**26**, 1689(1982).

35) F. Birch: J. Geophys. Res., **57**, 227(1952).

36) J. D. Thompson and J. M. Lawrence: Handbook on the Physics and Chemistry of Rare Earths, ed. K. A. Gschneidner, Jr. and L. Eyring (Elsevier, Amsterdam, 1994) Vol. 19, p. 383.

37) T. Kagayama, K. Suenaga, G. Oomi, Y. Onuki and T. Komatsubara: J. Magn. Magn. Mater., **90 & 91**, 451(1990).

38) F. F. Voronov, V. A. Goncharova, and O. V. Stal'gorova: Sov. Phys. JETP, **49**, 687(1979).

39) M. J. Besnus, A. Braghta, N. Hamdaoui and A. Meyer: J. Magn. Magn. Mater., **104–107**, 1385(1992).

40) H. Yashima, H. Mori, N. Sato, T. Satoh and K. Kohn: J. Magn. Magn. Mater., **31–34**, 411(1983).

41) J. Rossat–Mignod, L. P. Pegnault, J. L. Jacoud, C. Vettier, P. Lejay, J. Flouquet, E. Walker, D. Jaccard, A. Amoto: J. Magn. Magn. Mater., **76 & 77**, 376(1988).

42) K. Hanzawa, K. Yamada, K. Yosida: J. Magn. Magn. Mater., **47 & 48**, 357(1985).

43) A. J. Millis, Phys. Rev. B**48**, 7183(1993).

44) A. Yoshimori and H. Kasai, J. Magn. Magn. Mater., **31–34**, 475(1983).

45) T. Kagayama and G. Oomi in Proceeding of the Hiroshima Workshop on Transport and Thermal Properties of f–electron systems, edited by G. Oomi, H. Fujii and T. Fujita

(Plenum, New York, 1993), p. 155.

46) D. L. Cox: Physica B **186–188**, 312(1993).

47) S. Quezel, P. Burlet, J. L. Jacoud, L. P. Regnault, J. Rossat–Mignod, C. Vettier, P. Lejiay and J. Flouquet: J. Magn. Magn.Mater. **76 & 77**, 403(1988).

48) T. Pietrus, B. Bogenberger, S. Mock, M. Sieck, H. v. Löhneysen: Physica B **206 & 207**, 317(1995).

49) K. Kadowaki and S. B. Woods: Solid State Commun., **58**, 507(1986).

50) H. U. Desgranges and K. D. Schotte, Phys. Lett. **A91**, 240(1982).

51) J. Rossat–Mignod, L. P. Regnault, J. L. Jacoud, C. Vettier, P. Flouquet, E. Walker, D. Jaccard and A. Amato: J. Magn. Magn.Mater. **76 & 77**, 376(1988).

公　表　論　文

(1) Transition from Magnetic to Nonmagnetic Ground State in a Heavy-Fermion Compound Ce_7Ni_3 under High Pressure

K. Umeo, H. Kadomatsu and T. Takabatake

Physical Review, B**54**, 1194-1198(1996).

(2) Pressure Effect on the Low Temperature Specific Heat and Magnetic Susceptibility of Heavy Fermion Compound Ce_7Ni_3

K. Umeo, K. Ishii and H. Kadomatsu

Journal of Magnetism and Magnetic Materials, **148**, 409-412(1995).

(3) Electrical Resistivity of Ce_7Ni_3 under Pressure

K. Umeo, K. Ishii and H. Kadomatsu

Solid State Communications, **90**, 321-324(1994).

参 考 論 文

(1) External Pressure Enhancement of the Dense Kondo Effect in a PdCe Intermetallic Compound

K. Umeo, Y. Aya, M. Itakura, N. Kuwano and K. Oki

Journal of Physics and Chemistry of Solids, **54**, 131–134(1993).

(2) Variations in Lattice Parameters with Annealing Temperature for L–Pd_5Ce

N. Kuwano, K. Umeo, K. Yamamoto, M. Itakura and K. Oki

Journal of Alloys and Compounds, **181**, 61–68(1992).